RSC Advances

PAPER

View Article Online
View Journal | View Issue

Cite this: *RSC Adv.*, 2024, **14**, 10304

Exploitation of the multitarget role of new ferulic and gallic acid derivatives in oxidative stress-related Alzheimer's disease therapies: design, synthesis and bioevaluation†

Fahad Hussain,[a] Ayesha Tahir,[a] Muhammad Saeed Jan,[b] Noor Fatima,[a] Abdul Sadiq[c] and Umer Rashid *[a]

Monoamine oxidases (MAOs) inhibitors could decrease reactive oxygen species (ROS) generation, enhance mono-aminergic neural transmission, and have major therapeutic benefits for the treatment of Alzheimer's disease (AD). Following the conjunction of ferulic acid (FA)/gallic acid (GA) with sulfonamide, alanine and 2-aminobenzothiazole, we planned to assess the radical scavenging and antioxidant properties of synthesized analogs by using 2,2-diphenyl-1-picrylhydrazyl (DPPH), 2,2′-azino-bis(3-ethylbenzothiazoline-6-sulfonic acid) (ABTS) and ferric ion reducing antioxidant power (FRAP) assays. GA analog **28** was identified as the most potent antioxidant compound with IC_{50} values of 1.77 μM and 2.06 μM in DPPH and ABTS assays respectively. In the *in vitro* enzyme inhibition assays, synthesized derivative **23** emerged as a potent multitarget inhibitor of hMAO-B, eeAChE. COX-2 and 5-LOX with IC_{50} values of 0.037 μM, 0.071 μM, 14.3 μM and 0.59 μM, respectively. Moreover, selected compounds **23**, **25**, **26** and **28** displayed good to moderate inhibition of self-mediated amyloid β_{1-42} peptide aggregation. More importantly, compounds **23**, **25**, **28** and **29** showed no neurotoxicity on SH-SY5Y cells and also showed excellent neuroprotective effects against H_2O_2-induced SH-SY5Y cells. In the *in vivo* experiment, antioxidant enzymes superoxide dismutase (SOD), catalase and glutathione peroxidase (GSH-Px) were studied in the brain of male BALB/c mice at the dose of 5 mg kg^{-1}. All the tested compounds, except **29**, have shown good to *in vivo* antioxidant potential. Docking studies on 3D crystallographic structures of AChE and MAO-B showed significant interactions with catalytic amino acid residues. In conclusion, the current study showed that FA/GA derivatives could be further exploited for their multitarget role in oxidative stress-related AD therapies.

Received 30th January 2024
Accepted 20th March 2024

DOI: 10.1039/d4ra00766b

rsc.li/rsc-advances

Introduction

Neurodegeneration is an inflammatory disorder that results in the gradual loss of neural function, resulting in cognitive deficit, memory loss, and various types of ataxias.[1] This feature plays a role in diseases such as Epilepsy, Parkinson's disease (PD), Alzheimer's disease (AD), and Huntington's disease (HD). Neurodegenerative diseases affect millions of people worldwide. So, it imposes a significant social and economic risk to our society, particularly in low- and middle-income nations.[2–5]

The most frequent neurodegenerative disorder is AD. It appears to be a multifaceted progressive aged-dependent neurophysiological condition that has yet no medical treatment that can completely halt its progression. In 2018, there were over 50 million AD sufferers globally, and in the next 30 years, that figure is predicted to quadruple.[6] Extracellular deposition of amyloid-β (Aβ) plaques inflammation, neurofibrillary tangles (NFTs) with hyperphosphorylation of tau protein intracellularly, oxidative stress (OS), synaptic and neuronal loss are all symptoms of AD.[7,8]

As many efforts and resources are already committed to AD research over many years but there is no viable medicine that can decrease or completely stop its effects. The available drugs for AD only had symptomatic relief with moderate efficacy.[9–11] Unfortunately, only cholinergic targets have shown any benefit among the several therapy options for AD. According to this view, decreased levels of ACh encourage memory loss and cognitive impairment in the brain. There are four medicines approved for AD (donepezil, galantamine, memantine, and rivastigmine) by the FDA. Out of these four three are cholinesterase inhibitors (ChEI), which are FDA-approved for AD. The

[a]*Department of Chemistry, COMSATS University Islamabad, Abbottabad Campus, 22060 Abbottabad, Pakistan. E-mail: umerrashid@cuiatd.edu.pk*
[b]*Department of Pharmacy, Bacha Khan University, 24420, Charsadda, KPK, Pakistan*
[c]*Department of Pharmacy, University of Malakand, 18000 Chakdara, KP, Pakistan*

† Electronic supplementary information (ESI) available. See DOI: https://doi.org/10.1039/d4ra00766b

need for novel medicines that can delay or stop the progress of AD is both significant and urgent.[12]

Overall, acetylcholine esterase (AChE), monoamine oxidases (MAOs), beta-secretase 1 (BACE-1), metal ions in the nervous system, histamine receptor-third subtype (the H3 receptor), glycogen synthase kinase-3 beta (GSK-3β), phosphodiesterases (PDEs), 5-hydroxytryptamine (5-HT) receptors, and *N*-methyl-D-aspartate (NMDA) receptor are major biological targets. These receptors and their associated pathways of signalling may impact AD drug development.[13] AD is caused by decreased synthesis of an important neurotransmitter in the brain known as acetylcholine which leads to progressive cognitive impairment and defective quality of life. Acetylcholinesterase (AChE) is the enzyme which is particularly responsible for hydrolysing acetylcholine to acetate and choline. The primary causes of the reduction in cognitive function in AD patients are the degradation of cholinergic neurons and the loss of neural transmission.[14] Cognitive improvement has been observed by inhibiting the AChE which is responsible for the disintegration of acetylcholine.[15–18] Hence, AChE is a significant therapeutic target related to AD, so multi-target design approaches could be utilized for the inhibition of AChE.[19]

Another main factors causing axonal breakdown and the death of neuronal cells is neuroinflammation (NI). The metabolic process that produces prostaglandins and leukotrienes from arachidonic acid (AA) aids in the modulation of NI. It is widely known that cyclooxygenase and lipoxygenase (COX and LOX), which produce inflammatory mediators including cytokines and leukotrienes and aid in modulating NI. Neurodegenerative diseases cause an increase in COX-2 expression in neurons and glial cells. While, 5-lipoxygenase (5-LOX) is essential for the production of leukotrienes from AA. An increasing amount of research indicates that the proinflammatory protein enzyme (5-LOX) has a significant role in modulating the emergence of age-related neuropathology. Additionally, the brain of AD has elevated lipoxygenase (LOX) expression, which has been linked to elevated tau phosphorylation and Aβ production. Inhibition of 5-LOX activation can delay the onset and/or slow down the course of age-related brain disorders.[3,15]

Reactive oxygen species (ROS) generation is known to be significantly influenced by types A and B of monoamine oxidases (MAOs), which catalyse the metabolic oxidation of monoamine neurotransmitters. Under normal circumstances, monoamine oxidase A (MAO-A), which is mostly located in catecholaminergic neurons, regulates dopamine levels.[20] However, monoamine oxidase B (MAO-B) rises in glial cells and takes over as the main enzyme to metabolize dopamine when neuronal degeneration occurs in AD.

ROS are produced when ground state O_2 and dopamine are broken down by MAO-B. This process results in oxidative stress. This yields 3,4-dihydroxyphenylacetaldehyde, an ammonium molecule, and hydrogen peroxide (H_2O_2), which forms hydroxyl radicals when it combines with the iron ion (Fe^{2+}) in dopaminergic neurons.[21] This is resulted in oxidative stress (OS) and the death of neural cells. Therefore, inhibitors of monoamine oxidase-B (MAO-B) increase levels of dopamine in addition to producing neuroprotective benefits by reducing the generation of ROS.[22] Thus, blocking MAO-B appears to be a viable treatment option for AD symptoms. MAO-B bioactivity is greatly elevated in the hippocampal and cerebral cortex areas of patients with AD, accounting for over 80% of total MAOs activity in the central nervous system. MAO-B inhibitors could decrease ROS production (oxidative stress), enhance mono-aminergic neural transmission, and have major therapeutic benefits such as antioxidation, cognitive improvement, and neural protection, which could be useful in case of AD.[23–25]

The amyloid cascade hypothesis suggests that the formation of aggregation and misfolding of amyloid beta (Aβ) peptide play a critical role in developing the extracellular amyloid plaques which is the causative agent of Alzheimer's pathology.[1] Hence, the accumulation of Aβ is observed as a primary cause for the development of AD. Literature studies revealed that Aβ and oxidative stress (OS) are interlinked as Aβ can induce OS resulting in an increase in Aβ deposition.[26]

Ferulic acid (FA) is *trans*-4-hydroxy-3-methoxycinnamic acid and possess many pharmacological effects including antioxidant, antifibrosis, and anti-inflammation and it also protects the vascular endothelium. In respect of antioxidants, either they remove the ROS, that is present in excessive amounts or they may also directly interact with free radicals for their removal.[27,28] Due to its promising antioxidant and anti-inflammatory effects, ferulic acid has been considered as a potential neuroprotective therapy against AD, taking into account the pathophysiological framework of the disease. Lan *et al.* designed and synthesized compounds of FA. The compounds were synthesized based on the antioxidant and anti-inflammatory properties of FA, which can aid in the disaggregating impact of Aβ and inhibit AChE and BChE.[29] Ester derivative of ferulic acid **1** (Fig. 1) showed strong antioxidant activity (1.26 equivalent to Trolox), 49.2% reduction of Aβ aggregation at 20 μM, and cholinesterase inhibition (IC_{50} 19.7 nM for AChE and 0.66 μM for BChE). Additionally, the molecule showed BBB penetration and neuroprotective activity. *O*-Alkylamine derivatives of FA have been synthesized by Sang *et al.* The compound (**2**, Fig. 1) exhibited exceptional inhibitory efficacy against MAO-A and MAO-B, with IC_{50} values of 6.3 and 8.6 μM, respectively, and BChE inhibitory action with an IC_{50} value of 8.9 nM. It demonstrated strong antioxidant activity (ORAC = 0.52 eq.) and neuroprotective properties against SH-SY5Y neurotoxicity induced by $A\beta_{1-42}$. In 2022, Xian *et al.*, synthesized compound (**3**, Fig. 1) a dimeric FA

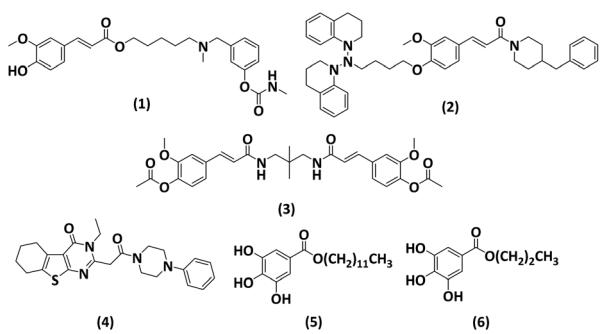

Fig. 1 Structures of reported derivatives.[29–34]

analogue with a diamide linker, which demonstrated strong inhibition of AChE (IC_{50}, 0.35 μM) and excellent suppression of Aβ aggregation (46.6% at 20 μM).[30] Other than FA Eissa *et al.*, reported compound (**4**, Fig. 1) containing thienopyrimidine as multipotent framework for the AChE (IC_{50} = 0.07 μM), BuChE (IC_{50} = 0.059 μM) and $A\beta_{42}$ (IC_{50} = 2.081 μM) with significant antioxidant activity.[31]

Gallic acid (GA) is a tri-phenolic secondary metabolite present in plants or tannins parts, having low molecular weight. They are hydroxybenzoic acids, present in tea leaves, oak bark, blackberry, sumac, *Caesalpinia mimosoides*, gallnuts, and witch hazel. GA has a wide range of biological actions, including antioxidants, anti-inflammatory, antiviral, antimicrobial, anticarcinogenic, and also against neurodegenerative diseases. Throughout the plant world, GA and its derivatives, including lauryl gallate (**5**), and propyl gallate (**6**), as shown in Fig. 1, are phenolic acids found in plant metabolites. The length of the carbon chains bonded to the carboxyl group varies among its derivatives. Reports on the medical applications of GA, including its antibacterial, anti-allergy, anti-inflammatory, and oxidative stress properties, are varied. To avoid excessive inflammatory reactions, GA may downregulate the production of pro-inflammatory and inflammatory mediators such as interleukin, tumour necrosis factor-α (TNF-α), interferon-γ (IFN-γ), cyclooxygenase-2 (COX-2), and nuclear factor κB (NF-κB). Above all, GA is a potent antioxidant that can be utilized to protect human cells from both acute and long-term oxidative stress, which makes it a valuable candidate for use as a therapeutic agent.[32–34]

Materials and methods

General

The reactants and solvent were acquired from Sigma Aldrich including FA, GA and N-Boc–alanine. Bruker 400 MHz spectrometers were used for the ^{1}H NMR and ^{13}C NMR having TMS as internal reference. The melting point apparatus (Stuart SMP10) was used for the determination of the melting points of synthesized compounds. The progress of the reaction was monitored with the help of TLC with silica gel 60F24 in pre-coated form. The Elemental analysis of compounds was also carried out (±0.4% of the measured values), Elemental Vairo CHN analyzer (EI III) was utilized for the elemental analysis. The purity of the final products was evaluated by utilizing the HPLC Shimadzu system having column C18 RP and its system was isocratic at RT. The purity of biologically active compounds was greater than 95%, which was determined by using the HPLC. The liquid chromatography (high-performance) which contains LCMS (ion trapped) G2445D SL and diode array detector (DAD) G1315 was used to obtain images of liquid chromatography (LC-MS).

General method for synthesis for amide derivative of alanine (12)

A mixture of N-Boc-protected alanine (**9**, 10 mmol) and thionyl chloride (12 mmol) was stirred in anhydrous DCM at 0 °C to yield its chloride **10**, after that DCM and thionyl chloride was evaporated at room temperature. The stirring was continued by the addition of ammonium acetate and acetone as a solvent in the reaction mixture to yield the amide form of Boc-protected alanine (**11**) in the form of precipitates that were filtered and recrystallized with ethanol. The product (**11**) was de-protected in the presence of CF_3COOH in DCM under a nitrogen environment to yield the amide derivative (**12**) of alanine in the form of precipitates there filtered and recrystallized with ethanol. All the proceedings of reaction till the last step were monitored by the help of TLC.

^{1}H NMR (400 MHz, $CDCl_3$) δ 6.31 (s, 2H), 5.01 (d, J = 5.5 Hz, 2H), 3.96 (h, J = 5.3 Hz, 1H), 1.38 (s, 3H); ^{13}C NMR (100 MHz, $CDCl_3$) δ 175.9, 50.6, 18.5.

General method for synthesis for ferulic acid derivative (14)

A mixture of FA and benzyl bromide in ACN was stirred under reflux for almost 12 h, after the completion of reaction (monitored by TLC), the FA derivative (**14**) was purified by the help of column chromatography.

(*E*)-3-(4-(Benzyloxy)-3-methoxyphenyl)acrylic acid (14)

^{1}H NMR (400 MHz, $CDCl_3$) δ 9.94 (s, 1H), 7.65 (d, J = 16.6 Hz, 1H), 7.41 (ddt, J = 6.5, 1.6, 0.9 Hz, 2H), 7.38–7.35 (m, 1H), 7.35–7.26 (m, 2H), 7.15–7.10 (m, 2H), 6.93 (dt, J = 8.3, 1.0 Hz, 1H), 6.34 (d, J = 16.7 Hz, 1H), 5.17 (t, J = 0.9 Hz, 2H), 3.87 (s, 3H); ^{13}C NMR (100 MHz, $CDCl_3$) δ 169.55, 150.82, 145.92, 145.24, 136.03, 128.50 (2), 128.25, 128.16, 127.71 (2), 124.14, 117.62, 115.60, 111.90, 71.06, 56.02; analysis calculated for $C_{17}H_{16}O_4$, C, 71.82; H, 5.67; O, 22.51; observed: C, 71.74; H, 5.69.

General method for synthesis for FA and cinnamic acid derivative (18–29)

To the solution of 20 mmol of FA derivatives (**FA**, **14–15**) and GA DCM under N_2 environment 1-hydroxy-benzotriazole (HOBt, 1.2 equiv.) 1-(3-dimethylaminopropyl)-3-ethylcarbodiimide hydrochloride (EDC·HCl, 1.2 equiv.), and Hunig's base (2.5 equiv.). It was allowed to stir for 5 minutes, after that amines (**12**, **16–17**, 20 mmol) were added in the reaction mixture and stirring was continued at room temperature. After the completion of the reaction (monitored by TLC) ethyl acetate was added in it, and washed with aq. HCl (0.6 M, 30 mL). Solvent extraction was carried out multiple times with ethyl acetate (60 mL each). The organic layers (ethyl acetate) were at the end mixed completely with the brine and saturated solution of sodium bicarbonate (20 mL each). After drying, it was filtered, and the organic solvent was removed through the vacuum evaporator. All of the synthesized products (**18–29**) were purified with the help of column chromatography having hexane and ethyl acetate system.

(*E*)-*N*-(1-Amino-1-oxopropan-2-yl)-3-(4-hydroxy-3-methoxyphenyl)acrylamide (18)

Off-white, yield = 79%, m.p. 201–203 °C; R_f = 0.51; (DCM/MeOH; 4 : 1); HPLC purity = 99% (C18 RP, MeOH/H_2O – 90 : 10), TR = 6.2 min. ^{1}H NMR (400 MHz, DMSO-d_6) δ 9.14 (s, 1H, OH), 8.09 (s, 1H, NH), 7.69 (d, 1H, J = 15.72 Hz, CH), 7.12 (d, 1H,

$J = 7.8$ Hz, ArH), 7.02 (d, 1H, $J = 7.8$ Hz, ArH), 6.89 (d, $J = 8.2$ Hz, 1H), 6.70 (d, 1H, $J = 15.72$ Hz, CH), 6.56 (s, 2H, NH_2), 3.83 (s, 3H, CH_3), 3.64 (q, $J = 5.48$ Hz, 3H), 1.26 (d, $J = 5.48$ Hz, 3H); ^{13}C NMR (100 MHz, DMSO-d_6) δ 174.5, 167.5, 149.7, 149.1, 141.1, 126.2, 123.1, 119.1, 115.8, 111.8, 56.3, 48.2, 17.4. Analysis calculated for $C_{13}H_{16}N_2O_4$, C, 59.08; H, 6.10; N, 10.60; O, 24.22; observed: C, 58.98; H, 6.12; N, 10.57.

(*E*)-*N*-(1-Amino-1-oxopropan-2-yl)-3-(4-(benzyloxy)-3-methoxyphenyl)acrylamide (19)

Off-white solid, yield = 73%, m.p. 232–234 °C; $R_f = 0.55$; (DCM/MeOH; 8 : 1); HPLC purity = 98.4% (C18 RP, MeOH/H_2O – 90 : 10), TR = 7.5 min. ^{1}H NMR (400 MHz, DMSO-d_6) δ 8.06 (s, 1H, NH), 7.69 (d, 1H, $J = 15.88$ Hz, CH), 7.19–7.16 (m, 3H, ArH), 7.12–7.07 (m, 4H, ArH), 7.01–6.98 (m, 1H, ArH), 6.70 (d, 1H, $J = 15.72$ Hz, CH), 6.56 (s, 2H, NH_2), 5.27 (s, 2H, OCH_2), 3.82 (s, 3H, CH_3), 3.65 (q, $J = 5.40$ Hz, 3H), 1.26 (d, $J = 5.40$ Hz, 3H); ^{13}C NMR (100 MHz, DMSO-d_6) δ 174.6, 167.5, 151.6, 146.1, 140.4, 137.4, 130.8, 129.7, 128.8, 127.8 (2), 125.9 (2), 119.6, 115.2, 111.5, 71.1, 56.2, 48.2, 17.4. Analysis calculated for $C_{20}H_{22}N_2O_4$, C, 67.78; H, 6.26; N, 7.90; O, 18.06; observed, C, 67.88, H, 6.24, N, 7.88.

(*E*)-3-([1,1′-Biphenyl]-4-yl)-*N*-(1-amino-1-oxopropan-2-yl)acrylamide (20)

Yellow oil, yield = 75%, $R_f = 0.57$; (DCM/MeOH; 8 : 1); HPLC purity = 98.2% (C18 RP, MeOH/H_2O – 90 : 10), TR = 8.1 min. ^{1}H NMR (400 MHz, DMSO-d_6) δ 8.07 (d, 1H, $J = 5.52$ Hz, NH), 7.79–7.73 (m, 4H, ArH), 7.68 (d, 1H, $J = 15.68$ Hz, CH), 7.46–7.40 (m, 3H, ArH), 7.35–7.31 (m, 1H, ArH), 7.18 (d, 1H, ArH), 6.71 (d, 1H, $J = 15.68$ Hz, CH), 6.57 (s, 2H, NH_2), 3.65 (q, $J = 5.44$ Hz, 3H), 1.26 (d, $J = 5.44$ Hz, 3H); ^{13}C NMR (100 MHz, DMSO-d_6) δ 174.6, 167.8, 144.9, 143.2, 137.5, 134.7, 129.1 (2), 128.9 (2), 127.5, 126.7 (2), 126.0 (2), 118.5, 48.3, 17.6. Analysis calculated for $C_{18}H_{18}N_2O_2$, C, 73.45; H, 6.16; N, 9.52; O, 10.87; observed, C, 73.36, H, 6.18, N, 9.51.

(*E*)-3-(4-Hydroxy-3-methoxyphenyl)-*N*-(6-hydroxybenzo[*d*]thiazol-2-yl)acrylamide (21)

Dark yellow solid, yield = 59%, m.p. 259–261 °C; $R_f = 0.49$; (*n*-hexane/EA; 3 : 1); HPLC purity = 98.7% (C18 RP, MeOH/H_2O – 90 : 10), TR = 10.5 min. ^{1}H NMR (400 MHz, DMSO-d_6) δ 9.16 (s, 1H, OH), 8.32 (s, 1H, NH), 8.17 (d, $J = 7.8$ Hz, 1H), 7.68 (d, 1H, $J = 15.6$ Hz, CH), 7.17–7.14 (m, 1H), 7.10 (d, 1H, $J = 7.8$ Hz, ArH), 7.04 (d, 1H, $J = 7.8$ Hz, ArH), 6.86 (d, $J = 8.2$ Hz, 1H), 6.79 (d, $J = 7.84$ Hz, 1H), 6.71 (d, 1H, $J = 15.6$ Hz, CH); ^{13}C NMR (100 MHz, DMSO-d_6) δ 166.4, 157.6, 152.3, 149.4, 149.0, 144.9, 142.6, 132.4, 126.3, 123.1, 119.3, 118.8, 116.6, 114.5, 111.5, 107.7, 56.2. Analysis calculated for $C_{17}H_{14}N_2O_4S$, C, 59.64; H, 4.12; N, 8.18; O, 18.69; S, 9.36; observed, C, 59.76, H, 4.10, N, 8.21.

(*E*)-3-(4-(Benzyloxy)-3-methoxyphenyl)-*N*-(6-hydroxybenzo[*d*]thi-azol-2-yl)acrylamide (22)

Light yellow, yield = 59%, m.p. 234–236 °C; $R_f = 0.45$; (*n*-hexane/EA; 5 : 1); HPLC purity = 99.1% (C18 RP, MeOH/H_2O – 90 : 10), TR = 13.8 min. ^{1}H NMR (400 MHz, DMSO-d_6) δ 10.33 (s, 1H), 8.32 (s, 1H), 8.19 (d, 1H, $J = 8.8$ Hz, ArH), 7.90 (d, 1H, $J = 8.64$ Hz, ArH), 7.65 (d, 1H, $J = 15.56$ Hz, CH), 7.62–7.58 (m, 1H), 7.13–7.00 (m, 7H), 6.70 (d, 1H, $J = 15.60$ Hz, CH), 5.28 (s, 2H, CH_2), 3.82 (s, 3H, CH_3); ^{13}C NMR (100 MHz, DMSO-d_6) δ 168.1, 158.2, 153.8, 151.9, 144.9, 143.1, 141.9, 136.2, 131.9, 129.0, 128.4 (2), 127.1 (2), 126.2, 123.2, 119.0, 116.8, 112.5, 112.3, 110.9, 105.4, 73.7, 57.1. Analysis calculated for $C_{24}H_{20}N_2O_4S$, C, 66.65; H, 4.66; N, 6.48; O, 14.80; S, 7.41; observed, C 66.54, H, 5.64, N, 6.47.

(*E*)-3-([1,1′-Biphenyl]-4-yl)-*N*-(6-hydroxybenzo[*d*]thiazol-2-yl) acryl-amide (23)

Yellow solid, yield = 66%, m.p. 223–225 °C; $R_f = 0.43$; (*n*-hexane/EA; 5 : 1); HPLC purity = 100% (C18 RP, MeOH/H_2O – 90 : 10), TR = 12.2 min. ^{1}H NMR (400 MHz, DMSO-d_6) δ 10.31 (s, 1H), 8.34 (s, 1H), 8.20 (d, 1H, $J = 7.8$ Hz, ArH), 7.83 (d, 2H, $J = 8.44$ Hz, ArH), 7.71 (d, 2H, $J = 8.44$ Hz, ArH), 7.67 (d, 1H, $J = 15.6$ Hz, CH), 7.15–7.12 (m, 1H), 6.77 (d, 2H, $J = 8.44$ Hz, ArH), 6.70 (d, 1H, $J = 15.60$ Hz, CH); ^{13}C NMR (100 MHz, DMSO-d_6) δ 166.4, 157.0, 152.2, 144.9, 142.8, 140.0, 135.7, 134.9, 131.7, 129.5 (2), 129.0 (2), 128.3 (2), 127.5, 126.2 (2), 119.9, 119.0, 114.5, 107.7. Analysis calculated for $C_{22}H_{16}N_2O_2S$, C, 70.95; H, 4.33; N, 7.52; O, 8.59; S, 8.61; observed, C, 70.86, H, 4.35, N, 7.55.

(*E*)-3-(4-Hydroxy-3-methoxyphenyl)-*N*-(4-sulfamoylphenyl) acryl-amide (24)

Yellow solid, yield = 76%, m.p. 241–243 °C; $R_f = 0.48$; (DCM/MeOH; 8 : 1); HPLC purity = 97.8% (C18 RP, MeOH/H_2O – 90 : 10), TR = 12.7 min. ^{1}H NMR (400 MHz, DMSO-d_6) δ 9.74 (s, 1H, NH), 9.16 (s, 1H, OH), 7.89 (d, 2H, $J = 8.4$ Hz, ArH), 7.67 (d, 1H, $J = 15.72$ Hz, CH), 7.54 (d, 2H, $J = 8.4$ Hz, ArH), 7.16 (d, 1H, $J = 8.2$ Hz, ArH), 7.11 (s, 1H, ArH), 7.04 (d, $J = 8.2$ Hz, 1H), 6.95 (s, 2H, NH_2), 6.71 (d, 1H, $J = 15.72$ Hz, CH), 3.84 (s, 3H, CH_3); ^{13}C NMR (100 MHz, DMSO-d_6) δ 165.5, 149.4, 149.0, 143.2, 141.6, 136.2, 127.8 (2), 126.0, 123.1, 120.8, 120.6 (2), 116.0, 111.6, 56.6. Analysis calculated for $C_{16}H_{16}N_2O_5S$, C, 55.16; H, 4.63; N, 8.04; O, 22.96; S, 9.20; observed, C, 55.26, H, 4.61, N, 8.05.

(*E*)-3-(4-(Benzyloxy)-3-methoxyphenyl)-*N*-(4-sulfamoylphenyl) acrylamide (25)

Light yellow solid, yield = 70%, $R_f = 0.52$; (DCM/MeOH; 10 : 1); HPLC purity = 98.9% (C18 RP, MeOH/H_2O – 90 : 10), TR = 10.3 min. ^{1}H NMR (400 MHz, DMSO-d_6) δ 9.75 (s, 1H, NH), 7.77 (d, 2H, $J = 8.4$ Hz, ArH), 7.67 (d, 1H, $J = 15.72$ Hz, CH), 7.55 (d, 2H, $J = 8.4$ Hz, ArH), 7.13–7.06 (m, 6H, ArH), 7.02 (d, 1H, $J = 7.8$ Hz, ArH), 6.88 (d, $J = 8.2$ Hz, 1H), 6.96 (s, 2H, NH_2), 6.73 (d, 1H, $J = 15.72$ Hz, CH), 5.29 (s, 2H, OCH_2), 3.82 (s, 3H, CH_3); ^{13}C NMR (100 MHz, DMSO-d_6) δ 165.6, 151.6, 145.9, 142.9, 140.4, 137.4, 137.3, 130.8 (2), 129.8, 128.6, 127.9 (2), 127.1 (2), 124.1, 121.6 (2), 120.3, 115.6, 111.8, 71.6, 56.2. Analysis calculated for $C_{23}H_{22}N_2O_5S$, C, 63.00; H, 5.06; N, 6.39; O, 18.24; S, 7.31; observed, C, 65.10, H, 5.04, N, 6.40.

(*E*)-3-([1,1′-Biphenyl]-4-yl)-*N*-(4-sulfamoylphenyl)acrylamide (26)

Light yellow solid, yield = 61%, $R_f = 0.54$; (DCM/MeOH; 10 : 1); HPLC purity = 98.3% (C18 RP, MeOH/H_2O – 90 : 10), TR =

11.8 min. ^{1}H NMR (400 MHz, DMSO-d_6) δ 9.74 (s, 1H, NH), 7.86 (d, 2H, J = 8.40 Hz, ArH), 7.72 (d, 2H, J = 8.40 Hz, ArH), 7.68 (d, 1H, J = 15.6 Hz, CH), 7.48–7.43 (m, 3H, ArH), 7.33–7.30 (m, 1H, ArH), 7.16 (d, 1H, ArH), 6.99 (s, 2H, NH_2). 7.84–7.78 (m, 2H), 7.78–7.69 (m, 4H), 7.67–7.61 (m, 2H), 7.61–7.55 (m, 2H), 7.54–7.48 (m, 1H), 7.48–7.41 (m, 2H), 7.41–7.33 (m, 1H), 6.71 (d, J = 16.1 Hz, 1H); ^{13}C NMR (100 MHz, DMSO-d_6) δ 165.8, 142.3, 139.2, 138.1, 135.0, 134.2, 131.9, 129.8 (2), 129.3 (2), 128.5 (2),128.0, 127.6 (2), 126.5 (2), 120.6, 120.3 (2). Analysis calculated for $C_{21}H_{18}N_2O_3S$, C, 66.65; H, 4.79; N, 7.40; O, 12.68; S, 8.47; observed, C, 66.76, H, 4.81, N, 7.42.

N-(1-Amino-1-oxopropan-2-yl)-3,4,5-trihydroxybenzamide (27)

White solid, yield = 55%, R_f = 0.41; (DCM/MeOH; 4 : 1); HPLC purity = 98.8% (C18 RP, MeOH/H_2O – 95 : 5), TR = 6.4 min. ^{1}H NMR (400 MHz, DMSO-d_6) δ 9.11 (s, 2H, OH), 8.17 (s, 1H, OH), 7.89 (d, J = 5.96 Hz, 1H), 7.51 (s, 2H, ArH), 6.67 (s, 2H, NH_2), 4.36–4.29 (m, 1H); ^{13}C NMR (100 MHz, DMSO-d_6) δ 174.4, 167.9, 147.5 (2), 136.5, 127.7, 108.6 (2), 48.1, 17.6. Analysis calculated for $C_{10}H_{12}N_2O_5$, C, 50.00; H, 5.04; N, 11.66; O, 33.30; observed, C, 49.9, H, 5.02, N, 11.69.

3,4,5-Trihydroxy-*N*-(6-hydroxybenzo[*d*]thiazol-2-yl)benzamide (28)

White solid, yield = 55%, R_f = 0.41; (DCM/MeOH; 4 : 1); HPLC purity = 99.2% (C18 RP, MeOH/H_2O – 95 : 5), TR = 7.2 min. ^{1}H NMR (400 MHz, DMSO-d_6) δ 10.32 (s, 1H, OH), 9.08 (s, 2H, OH), 8.81 (s, 1H, OH), 8.31 (s, 1H, NH), 8.19 (d, J = 7.8 Hz, 1H), 7.50 (s, 2H, ArH), 7.15–7.12 (m, 1H), 6.76 (d, J = 7.84 Hz, 1H); ^{13}C NMR (400 MHz, DMSO-d_6) δ 166.2, 159.8, 152.7, 147.3 (2), 145.9, 138.4, 131.5, 124.8, 119.0, 114.7, 108.4, 106.3 (2). Analysis calculated for $C_{14}H_{10}N_2O_5S$, C, 52.83; H, 3.17; N, 8.80; O, 25.13; S, 10.07; observed, C, 52.92, H, 3.15, N, 8.81.

3,4,5-Trihydroxy-*N*-(4-sulfamoylphenyl)benzamide (29)

White solid, yield = 55%, R_f = 0.41; (DCM/MeOH; 4 : 1); HPLC purity = 98.8% (C18 RP, MeOH/H_2O – 95 : 5), TR = 6.4 min. ^{1}H NMR (400 MHz, DMSO-d_6) δ 9.13 (s, 2H, OH), 8.16 (s, 1H, OH), 7.78 (d, 2H, J = 8.4 Hz, ArH), 7.55 (d, 2H, J = 8.4 Hz, ArH), 7.52 (s, 2H, ArH), 6.67 (s, 2H, NH_2); ^{13}C NMR (100 MHz, DMSO-d_6) δ 167.9, 147.5 (2), 141.0, 138.6, 136.5, 127.8 (2), 125.2, 120.1 (2), 106.4 (2). Analysis calculated for $C_{13}H_{12}N_2O_6S$, C, 48.15; H, 3.73; N, 8.64; O, 29.60; S, 9.89; observed, C, 48.26, H, 3.75, N, 8.66.

Antioxidant activity by using DPPH

The 1,1-diphenyl-2-picrylhydrazyl (DPPH) test quantifies the antioxidant's capacity to donate hydrogen, transforming the stable DPPH free radical into a reduced form. This may be assessed by quantifying the percentage of the solution's absorbance that decreases at 517 nm, which is followed by a color shift from violet to yellow and this color shift is due to the radical reaction with the tested compounds. The stock solution (10 mM) of DPPH was prepared by dissolving it in MeOH. The test sample was then diluted to 0.1 mM. The target molecules were dissolved in DMSO to yield a 10 mM stock solution. As test samples, this stock solution was diluted to five different concentrations. Trolox was utilized as the standard. On a 96-well plate, the experimental methodology was carried out. Each test well received 100 μL of the tested drug, and 100 μL of DPPH, and was shaken before being incubated for 30 minutes at room temperature in the dark. Subsequently, three parallel measurements of the absorbance at 517 nm were made with the help of a microplate reader. Graph Pad Prism 4.03 was used to calculate the IC_{50} values of the test substances. The reduction of DPPH was measured by this equation:

$$\text{Percentage reduction of DPPH} = X_0 - (X_1 - X_2)/X_0 \times 100.$$

where X_0 is DPPH and methanol solution's absorbance, X_1 is DPPH with compound solution's absorbance, and X_2 is the compound (without DPPH) solution's absorbance.[35]

Antioxidant activity by using ABTS radical cation

A 7 mM concentration of 2,2′-azino-bis-2-ethylbenz-thiazoline-6-sulfonic acid (ABTS) was prepared in distilled water. ABTS stock solution was reacted with 2.45 mM potassium persulfate (final concentration) to create radical cation ABTS ($ABTS^+$), which was then left to stand at room temperature for a minimum of eighteen hours in the absence of light. The 50 mM ABTS buffer having pH = 7.4 was diluted with the help of sodium phosphate. Test compounds and trolox were added individually to 150 μL of 100 μM ABTS solution at varying concentrations (50 mL of total volume). Following the addition of trolox and antioxidant compounds to the ABTS solution, the reactants are properly mixed. After 150 minutes of standing at 30 °C, the optical absorbance of ABTS at 415 nm was determined. The experimental outcomes were compared after each individual treatment was carried out three times.[36]

Antioxidant activity by using FRAP radical cation

The synthesized compounds were explored for their overall antioxidant ability using the reduction power (FRAP test). It determined the reducing power of compounds, it basically form blue coloured (Fe(II)–TPTZ) ferrous tripyridyl triazine complex from (Fe(III)–TPTZ) ferric tripyridyl triazine at low pH, which was the observe at 593 nm. $FeCl_36H_2O$ (10 mL), TPTZ (2,4,6-tripyridyl-*s*-triazine) having 10.0 mL concentration in acetate buffer (100 mL) having pH 3.6 were mixed to prepare the Fe(II)–TPTZ reagent. Sample solution (400.0 μL) and Fe(II)–TPTZ reagent (3 mL), they were incubated for 15 min at 37 °C. Ascorbic acid as standard, at 593 nm the absorbance was observed and measured. Ascorbic equivalent (mmol/100 g compound) was used to report the results.[36]

$$\text{Amount of ascorbic acid} = 3.99 \times 10^{-4}\ \text{mm},$$
$$\text{amount of sample} = 0.04\ \text{mg concentration of ascorbic acid}$$
$$(\text{mmol}/100\ \text{g of sample}) = \text{absorbance of sample at 593 nm} \times \text{standard} \times 100$$

SH-SY5Y neuroblastoma cell toxicity and neuroprotective effect on H_2O_2-induced oxidative toxicity

Neuroblastoma cells (SH-SY5Y) were evaluated by the MTT for the toxicity effect of the compounds by already reported methods. In

the presence of fetal bovine serum (FBS), streptomycin (100 U mL^{-1}), and penicillin (100 U mL^{-1}) at 37 °C having 5% CO_2 the SH-SY5Y cells in DMEM were cultured. Firstly 96 well plates were seeded with 10 000 SH-SY5Y cells (density), and after that, compounds (**23**, **25**, **27**, **28**, and **29**) along with the reference including donepezil, rasagiline, trolox, and compounds were also seeded into 96 well plates in different concentrations. After the incubation period of 24 h at 37 °C, MTT (20 mL) was also added in and it was left for the incubation period of 4 h at 37 °C. Subsequently, after the removal of the medium DMSO (200 mL) was added to dissolve the formazan crystal of MTT. At 570 nm wavelength, the absorbance of each well plate was measured and 630 nm wavelength as a reference, we used a microculture plate reader to test each well absorbance at a wavelength of 570 nm and with a reference wavelength of 630 nm.

Human neuroblastoma SH-SY5Y cells were treated with compounds **23**, **25**, **27**, **28**, and **29** along with the reference compounds donepezil, trolox, and rasagiline at different concentrations. In percentage, the cell viability was expressed with the control group (100%). After that, they were subjected to either medium or H_2O_2 (400 μM) for a further four hours. Subsequently, each well was treated with 20 μL MTT (5 mg mL^{-1}) for four hours, and DMSO was applied to dissolve the formazan crystals. A Thermo microplate reader was used to measure the absorbance at 490 nm. A percentage was used to represent the cell viability, with 100% being the control group.

Cholinesterases inhibition assay

The cholinesterase *in vitro* bioassay for the synthesized compounds was evaluated by the already reported protocols.[3] Ellman's assay method was used for the synthesized compounds for the inhibition of *Electrophorus electrcus* AChE and equine serum lyophilized BChE. The synthesized compound's stock solution was prepared having pH 8.0 with potassium phosphate buffer. A sufficient amount of Ellman's reagent (DTNB), synthesized compound, and both enzymes (eeAChE and eqBChE) having 0.03 U mL^{-1} were reacted by 30 °C pre-incubation for 10 minutes after that 1 mM ATCI or BTCI was added in it for the incubation period of 15 minutes. Triplicates of reading were taken and the plotting sample concentration verses inhibition IC_{50} were obtained.

MAO isoforms inhibition assays

MAO isoforms (human MAO-A and MAO-B from Thermo Fisher Scientific) inhibition assay was evaluated for all of the synthesized compounds. The substrates used for this assay were benzylamine and tyramine. The assay was carried out in a dark environment (black) by utilizing a 96-well plate test. The protocol for this assay was carried out by already reported method (fluorometric).[24]

Inhibition assay of cyclooxygenase-2 COX-2

The selected compounds were evaluated for the enzyme inhibition for cyclooxygenase-2 (COX-2).[3,10,37] Firstly, the enzyme was prepared 300 U mL^{-1} for COX-2 by the addition of cofactor at °C for 5 minutes. The cofactor solution contains hematin (0.1 mM), glutathione (0.9 mM) and TMPD (*N*,*N*,*N*,*N*-tetramethyl-*p*-phenylenediamine dihydrochloride) (0.24 mM) in Tris HCl buffer (0.1 M) having pH of 8.0. The 60 mL of enzyme solution and test sample (20 mL) having different concentrations (ranging from 31.25–1000 mg mL^{-1}) were sited at room temperature for 5 minutes. The reaction was commenced by introducing 20 mL having arachidonic acid (30 mM). The combination was then allowed to react for five minutes. At 570 nm the absorbance was evaluated by using spectrophotometer (UV-visible). After that, the percentage of COX-2 enzyme inhibition was computed using the absorbance value per unit of time. The IC_{50} value were measured by graphing the concentration of the sample against inhibition. The positive control for COX-2 was celecoxib used in this assay. The triplicate tests were carried out, and for each inhibitor the IC_{50} value was determined.

Inhibition assay of 5-lipoxygeases (5-LOX)

The selected compounds were evaluated for the enzyme inhibition for 5-lipoxygeases (5-LOX) by using already reported methods.[3,10] Different concentration of selected compounds were utilized during assay having range from 15.625 to 500 μg mL^{-1}. After that the solution (5000 U mL^{-1}) of enzyme 5-LOX was prepared. 40 mM of substrate linoleic acid was used, the phosphate buffer (50 mM) having pH 6.3 was also prepared. Firstly the 0.25 mL of phosphate buffer containing different concentration of compounds was incorporated with addition of 0.25 mL of 5-LOX enzyme, which was incubated at RT for about 5 minutes. Furthermore, the substrate linoleic acid (1 mL) was added to the mixture, next after some time at 234 nm the absorbance was evaluated. The triplicate tests were carried out, and for each inhibitor the IC_{50} value was determined. The IC_{50} value were measured by graphing the concentration of the sample against inhibition. The reference drug used in this assay was zileuton.

Cell viability assay on normal human embryonic HEK-293 cells model

MTT assay was employed in order to evaluate the selected compounds on HEK-293 cells (human embryonic cells) for their cytotoxicity potential. In this assay the formazan is formed from MTT reagent by the ability of the oxidoreductive enzyme (NADPH dependent) which is present in viable cells. This assay basically measured the reducing power of viable cells. The 5000 cells per well, overall in culture medium of 100 μL was left overnight in 96-well plate at optimum conditions. Furthermore, test samples having different concentration (5–100 mM) were added to the cells containing wells, after that they were left for about 24 hours. The DMSO was employed as control, after thatMTT reagent having concentration of 10 μL was added in each well, incubation for almost 4 hours was employed in multi-well plate reader before taking reading at 570 nm.

ThT fluorescence assay for self-mediated $A\beta_{1-42}$ aggregation

Using a ThT-based fluorescence method, the impact on amyloid beta (1–42) self-aggregation was evaluated. Initially, 5

millimolar $A\beta_{1-42}$ sample stock solutions were made by preparing them in DMSO and freezing them at −20 °C. The peptide was agitated in 50 millimolar phosphate buffer of pH = 7.4 with 100 mM sodium chloride for 10 hours at 37 °C (ultimate amyloid beta concentration = 100 micromolar) and incubated in the absence or presence of different concentrations of the main compounds. Following incubation, the dilutions of the 20 microlitre of the aforementioned solutions were prepared with 50 millimolar glycine-sodium hydroxide buffer of pH = 7.4 containing the 10 micromolar thioflavin T to provide a final volume = 200 microlitre. The fluorescence intensity was then calculated using the black microwell plates with 96 wells and a microplate reader (λ_{em} = 480 nm, λ_{exc} = 450 nm). The triplicate tests were carried out, and for each inhibitor the IC_{50} value was determined.

In vivo antioxidant potential

In the *in vivo* antioxidant assay, a total of forty (**40**) albino mice were taken in 5 groups each having 8 animals in a group. Distilled water (0.4 mL) was given to the control group (group 1). The dosage of 5 mg kg^{-1} of tested synthesized compounds (**23**, **25**, **28**, and **29**) was given to groups 2, 3, 4, and 5. All groups of animals were evaluated for any toxicity symptoms, any type of alterations, and death daily. The *in vivo* antioxidant activity was evaluated by obtaining blood by heart puncture (direct) during 24 h by succeeding the last dose.

Serum preparation

The mice were given anesthesia by using moderate chloroform, following that serum preparation was carried out by utilizing 5 mL syringe having 21G needle, it was employed for taking the sample of blood through cardiac puncture. In a nutshell, it includes: the extraction of serum at 2500 rpm centrifugation for almost 15 minutes was carried out after the coagulation of blood.

Lipid peroxidation (LPO) determination in serum

Superoxide dismutase (SOD) estimation

The SOD was estimated by using reported methods with some modifications.[38–40] The system of xanthine–xanthine oxidase was employed for generating superoxide flux in this procedure, which was furthermore evaluated at 550 mm. The presented results are in units of U mL^{-1}.

Estimation of catalase activity

Serum's catalase activity was determined by using the modified reported method.[38–41] In a nutshell, it includes: serum (10 μL), potassium phosphate buffer (2.80 mL, 50 mM) having 7.0 pH was added in a test tube. By the addition of H_2O_2 (0.1 mL, 30 mM) the reaction was initiated and at 250 nm using spectrophotometer the H_2O_2 decomposition rate was measured for almost 5 minutes. Molar extinction coefficient (0.041 mM^{-1} cm^{-1}) was utilized for the calculation of catalase activity.

Determination of GSH

The GSH activity was determined by the reported protocol with modifications.[38–42] Homogenizer was used for the homogenates of brain in the cold saline and the unsolvable was thrown away by employing it at 10 000 rpm centrifugation for almost 15 min (4 °C). The enzymatic reaction was initiated by the addition of H_2O_2 in the mixture containing reduced nicotinamide adenine dinucleotide phosphate, sodium azide, glutathione (reduced), and glutathione reductase. The absorbance was observed and measured at 340 nm. The unit per mg protein was used to express the activity.

Statistical data analysis

All the data values of tests are represented in mean (±S.E.M.), the triplicates were carried out. The positive control group was compared with test (bonferoni) by using GraphPad prism Software USA to do a two-way ANOVA. The *P* values under 0.05 were deemed significant during statistics evaluation. Mean ± SEM was employed for all test results which are represented as, with $n = 3$. Moreover, with *P* 0.05 was used for defining of results of statistical significance. The *P* values are contrasted with the reference drug, such as * = $P < 0.05$, ** = $P < 0.01$ and *** = $P <$ 0.001, ns; not significant.

Docking studies

The docking simulation studies were performed for the most potent, moderate, and least active compounds of the *in vitro* inhibition assay to correlate the results. The investigation was carried out on potential targets (AChE, MAO-A, and MAO-B) by utilizing the Molecular Operating Environment (MOE). The 3D crystallographic structure of enzyme and inhibitor complex for AChE and MAO-B was retrieved from the Protein Data Bank (PDB). The PDB codes for AChE, MAO-A, MAO-B, COX-2, and 5-LOX are 2CKM, 2Z5X, 2V5Z, 1CX2, and 6N2W. The 3-D structure of downloaded enzymes (AChE, MAO-A/B, COX-2, 5-LOX) and synthesized compounds were minimized in terms of energy and preparation by already reported methodology.[3,15]

MOE was used for the docking procedure in which the force field (Amber10EHT) was implemented. The minimization of energy with 3D protonation of enzymes was executed at 0.1 gradient. The structure of synthesized compounds was prepared by using the MOE, for that the minimization was executed at a gradient of 0.00001. The methodology of Triangular Matcher docking was used for the docking simulation of the compounds into the active site of the enzyme. The minimum energy of the conformation was obtained with the help of induced fit model docking. The energy of binding of ligand was ranked by the GBVI/WSA scoring. kcal mol^{-1} is the unit for this scoring function. The analysis of the docking results was evaluated by using the MOE and Discovery studio software program.

Results and discussion

Design rational

The aim is to identify the derivatives that have balanced even mild biological activities against multiple targets instead of

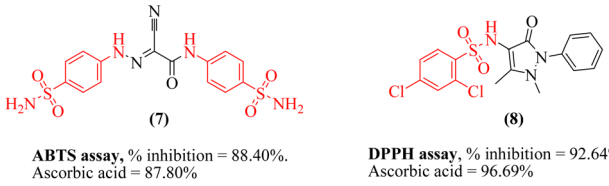

Fig. 2 Structures of reported antioxidant compounds with sulfonamide scaffold.

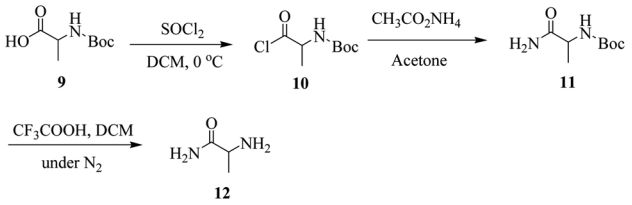

Scheme 1 Synthesis of amide derivative **12** of alanine.

finding one-target compound with high potency. Following the conjunction of FA and GA with sulfonamide, alanine, and 2-aminobenzothiazole, we planned to assess the radical scavenging and antioxidant properties of synthesized FA and GA analogs by using 2,2-diphenyl-1-picrylhydrazyl (DPPH), 2,2′-azino-bis(3-ethylbenzo-thiazoline-6-sulfonic acid) (ABTS) and ferric ion reducing antioxidant power (FRAP) assays. Thiazole and its derivatives present in coffee are reported to have antioxidant properties.[34–36,43] Moreover, benzothiazoles and phenolic acid compounds (FA and GA) have been found to exhibit potential antioxidant activity. The benzothiazole with aryl groups bearing hydroxy and methoxy groups exhibited significant antioxidant activity by the potential of free radicals scavenging. Thus, benzothiazole combination with the aryl group especially like phenolic acid could be beneficial scaffolds for the development of antioxidant agents.[44–47]

Sulfonamide (due to electron-donating species in the chemical structure) is considered as a valid scaffold for designing an antioxidant. Sulfonamides **7** and **8** has displayed antioxidant activities by having the potential to scavenge the free radicals and decrease oxidative stress (Fig. 2).[48,49]

Furthermore, our goal is to develop a framework that can increase neurotransmitter levels and prevent the formation of ROS by blocking the oxidative catabolism of monoamine neurotransmitters. The design of the framework was based on the active site constitution/volume of target biological macromolecules (Fig. S-1 to S-4 in the ESI†). Linear-type compounds like safinamide are considered suitable for MAO-B inhibition. The designed compounds in *trans*-isomeric form showed linearity. The alaninamide moiety was introduced to mimic the safinamide (a reversible and selective MAO-B inhibitor marketed drug). Our current research aims to address AD by employing a multitarget approach. To alleviate oxidative stress, we are targeting MAO-B. However, to combat the cholinergic deficit associated with the disease, we are focusing on inhibiting AChE. Additionally, by simultaneously addressing these multiple facets of AD, our approach seeks to provide a more comprehensive and effective treatment strategy for this complex condition. Inhibiting AChE leads to elevated levels of acetylcholine in the brain of AD patients, subsequently suppressing the aggregation of amyloid-beta. Moreover, recent research has shown that the inhibitors that interact with the peripheral anionic site of AChE also prevent Aβ aggregation and thus provide symptomatic relief to AD patients. The FA derivatives were designed by derivatization at hydroxyl group (–OH) at 4-position. While amide derivatives were planned by using sulfanilamide, alanine and 2-aminobenzothiazole. Similarly, amide derivative of GA were designed to increase the BBB permeation (Fig. 3). Trihydroxyl groups were left unchanged for antioxidant activity.

Chemistry

2-Aminopropanamide (amide derivative of alanine) was synthesized by using N-Boc-protected alanine **9** (Scheme 1). Acid chloride **10** of N-Boc-protected alanine **9** was synthesized by using thionyl chloride in DCM. Ammonium acetate ($CH_3CO_2NH_4$) were used to covert acid chloride into amide derivative **11**. Finally, deprotection of N-Boc to get final alaninamide **12** (Scheme 1).

To synthesize key intermediate **14**, FA was reacted with benzyl bromide (**13**) in acetonitrile under reflux conditions in 76% yield (Scheme 2).

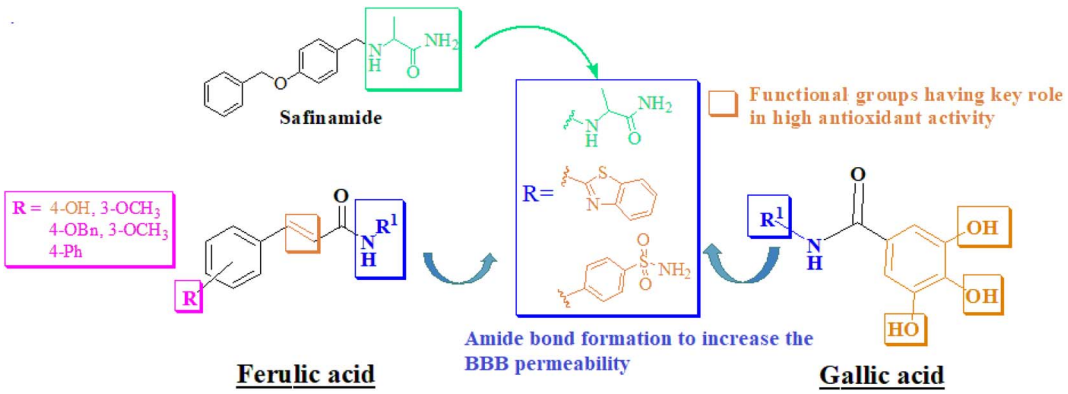

Fig. 3 Design rationale for current research.

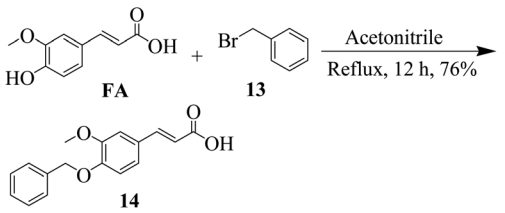

Scheme 2 Synthesis of benzyloxyphenyl derivative (**14**) of FA.

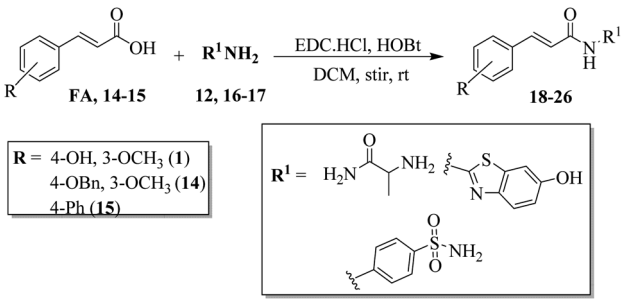

Scheme 3 Synthesis of amide derivatives of FA.

Finally, target compounds **18–26** and **27–29** were obtained by the condensation reaction of FA/its analogs (FA, **1**, **14–15**) and GA in the presence of 1-(3-dimethylaminopropyl)-3-ethylcarbodiimide hydrochloride (EDC·HCl) and hydroxybenzotriazole (HOBt) and DMAP. Compound **22** was in fact a cinnamic acid derivative we have selected to explore the role of methoxy group of FA. The obtained target compounds were purified using chromatographic technique. GA was used in amide bond reaction without acylating its hydroxyl groups. The resulting analogs were obtained in good yield (65–73%) (Schemes 3 and 4).

All the synthesized compounds were characterized by using spectroscopic (^{1}H/^{13}C-NMR) and chromatographic techniques (HPLC/LC-MS). Moreover, for further purity study, elemental analysis has also been performed. For biological screening, compounds should be >95% pure as determined by HPLC. Our compounds showed HPLC purity in the range of 97–100%/. Elemental analysis data should be provided to an accuracy within ±0.4%.[3]

Evaluation of radical scavenging and antioxidant properties

First of all, we assessed the radical scavenging and antioxidant properties of synthesized FA and GA analogs by using 2,2-diphenyl-1-picrylhydrazyl (DPPH), 2,2′-azino-bis(3-ethylbenzothiazoline-6-sulfonic acid) (ABTS) and ferric ion reducing antioxidant power (FRAP) assays. The results of the assays are presented in Table 1.

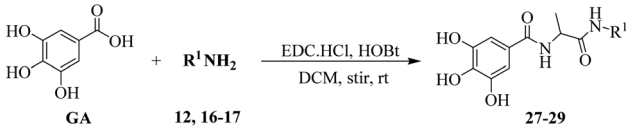

Scheme 4 Synthesis of amide derivatives GA.

The DPPH and ABTS assays are based on spectroscopic method based on quenching of stable coloured radicals (DPPH or ABTS$^{\bullet+}$).[50] These assay methods are used to assess the antioxidant capacities of the synthetic/natural products. The FRAP method is a non-specific colorimetric assay and is a putative index of reducing or antioxidant potential of compounds within the reach of every researcher working on oxidative stress. The assay has been carried out in a low pH buffer to reduce ferric tripyridyltriazine complex (Fe^{3+}–TPTZ) to ferrous (Fe^{2+}–TPTZ).[51] Our synthesized compounds showed excellent antioxidant activity in DPPH and ABTS assay. FA derivatives **21–23** and all the synthesized GA analogs (**27–29**) exhibited excellent activities. GA derivative **28** emerged as excellent antioxidant in both assays with IC_{50} values of 1.77 μM and 2.06 μM for DPPH and ABTS, respectively.

A FRAP experiment was used to measure the antioxidant capacity of all the tested samples based on their ability to transfer a single electron.[52] The FRAP values are presented as μM equivalent to the standard antioxidant ascorbic acid. The presence of FRAP values indicates that all of the compounds have well to moderate ferric reducing antioxidant ability. In the FRAP assay, the role of electron-donating and electron-withdrawing substituents is crucial in determining the antioxidant activity of a compound. Electron-donating substituents, such as hydroxyl (–OH), amino (–NH_2), and methoxy (–OCH_3) groups, can enhance the compound's ability to donate electrons, which is essential in the reduction of ferric ions to ferrous ions.[53] The compounds under evaluation have an overall antioxidant capability that is boosted by this electron-donating characteristic. While, the redox potential of compound and its capacity to function as a reducing agent in the FRAP test can be affected by electron-withdrawing substituents as carbonyl (C=O), sulfonamide (–SO_2NH_2) and nitro (–NO_2) groups. Electron-donating substituents like methoxy and benzyloxy groups can both be found on the *ortho*-position of the benzene ring, and their combined presence can increase the electron-donating capacity of the molecule. This improved ability to donate electrons is essential for the FRAP assay's conversion of ferric ions to ferrous ions, which increases the chemical under test's total antioxidant capacity. Similarly, biphenyl group present in our compounds has the capability to donate electron and thus increase the total antioxidant power.[54]

Although amide groups are not generally recognized for their direct antioxidant capabilities, they can, *via* a variety of indirect pathways, enhance a compound's total antioxidant capacity. For example, compounds containing amide groups may exhibit chelating properties, which can influence the redox reactions involved in the FRAP assay. Additionally, the presence of amide groups can affect the compound's overall chemical structure and electronic properties, which in turn may impact its ability to participate in redox reactions and donate electrons.[55]

Compounds **19**, **20**, **23** and **28** (Table 1) exhibited strong antioxidant activity. Compound **23** with biphenyl group and 6-hydroxy-benzothiazole core relatively emerged as excellent antioxidant with FRAP value of 53.57 μM. Whereas, benzyloxy- and biphenyl containing amides (**19** and **20**) has also shown

Table 1 Evaluation of antioxidant properties of synthesized compounds using DPPH, ABTS and FRAP assays

	IC_{50} (μM) ± SEM[a]		
Entry	DPPH	ABTS	FRAP value (μM)
18	58.34 ± 1.21	45.11 ± 1.77	29.84
19	81.34 ± 1.36	63.44 ± 1.14	40.61
20	<100	77.08 ± 1.37	44.81
21	14.44 ± 0.13	6.29 ± 0.09	36.01
22	16.33 ± 0.10	43.25 ± 1.34	ND
23	18.19 ± 0.11	12.11 ± 0.14	53.57
24	21.21 ± 0.15	48.80 ± 1.20	14.75
25	25.04 ± 1.16	20.73 ± 1.11	20.07
26	29.20 ± 1,15	40.59 ± 1.11	24.7
27	14.55 ± 0.52	20.37 ± 0.30	ND
28	1.77 ± 0.04	2.06 ± 0.11	45.24
29	10.84 ± 0.63	23.49 ± 1.04	ND
Ascorbic acid	4.89 ± 0.09	6.08 ± 0.21	90.89
Gallic acid	35.25 ± 1.04	35.25 ± 1.19	—
Ferulic acid	69.75 ± 1.48	35.25 ± 1.26	—

[a] ND = not determined.

good antioxidant activity. The inclusion of an electron withdrawing SO_2NH_2 resulted in low antioxidant activity. Compound **28** with GA (three hydroxyl groups) and 6-hydroxybenzothiazole core also emerged as excellent antioxidant with FRAP value of 45.24 μM.

Inhibition of ChEs

The inhibitory potential of the synthesized derivatives against ChEs (electric eel acetylcholinesterase (eeAChE) and equinebutrylcholinesterase (eqBChE)) was evaluated by using the modified Ellman method.[3] Donepezil was used as a reference drug. The results of inhibition of synthesized compounds are presented in Table 2. All the synthesized derivatives exhibited high selectivity towards eeAChE. 6-Hydroxy benzothiazole-biphenyl hybrid (cinnamic acid derivative **23**) emerged as the most potent eeAChE inhibitor with an IC_{50} value of 0.071 μM. FA derivatives (4-OH, 3-OCH_3 as R) with alaninamide, 6-hydroxy benzothiazole and sulfonamide as R1 (**18**, Fig. 3) showed good to poor eeAChE inhibition. Good to excellent AChE inhibition was displayed by derivatives (**19–20**, **22–23**, **25–26**) with hydrophobic groups (R = OBn and biphenyl). In FA series (**18–26**), all the other compounds exhibited eeAChE inhibition potential in low micromolar to submicromolar concentration except compound **18** (IC_{50} = 58.396 μM). In literature, a number of FA analogs have been reported for the treatment of AD. Lan, *et al.*, reported multitarget long chain ester derivatives of FA targeting hAChE, BChE, and self-induced $A\beta_{1-42}$ aggregation inhibition.[56] A number of compounds emerged as excellent multifunctional inhibitors. In another study, Zhipei *et al.*, synthesized amide and *O*-alkyl FA analogs using multitarget design strategy. Compounds displayed selectivity towards BChE (IC_{50} of TM-10 = 8.9 nM). Compounds also shown good potency towards MAO-A/B isoforms and self-induced $A\beta_{1-42}$ aggregation inhibition.[57] The results showed the GA analogues **27–29** were not able to show good eeAChE inhibition might be due to the less hydrophobic region in molecule and less linker length in these compounds to be accommodated in the active site of AChE. For eqBChE, only compounds **23**, **25**, **26** and **28** showed good (**26**) to moderate (**23**, **25** and **28**) inhibition.

Inhibition of MAO-A and MAO-B

Considering the importance of MAOs highly relevant to oxidative stress, we performed MAO-A and MAO-B inhibition assays.[24,58] A fluorescence-based protocol was carried out by

Table 2 Results of human MAO-A/MAO-B, and eeAChE/eqBChE and $A\beta_{1-42}$ peptide aggregation inhibition

	IC_{50} (μM) ± SEM[a]						
Compd no.	MAO-A	MAO-B	SI[b]	eeAChE	eqBChE	SI[b]	$A\beta_{1-42}$ peptide aggregation inhibition
18	na	10.043 ± 1.027	—	58.396 ± 0.09	na	—	—
19	89.546 ± 1.16	**0.318 ± 0.021**	281	15.241 ± 0.09	52.024 ± 1.422	3	—
20	10.028 ± 0.925	0.513 ± 0.070	19	13.510 ± 0.10	84.094 ± 1.318	6	—
21	37.118 ± 1.033	0.491 ± 0.024	75	29.837 ± 0.10	43.108 ± 1.09	1	—
22	19.403 ± 1.10	0.348 ± 0.041	55	0.172 ± 0.10	37.381 ± 1.17	217	—
23	**10.011 ± 0.50**	**0.037 ± 0.011**	**270**	**0.071 ± 0.10**	**15.638 ± 0.901**	**220**	*23.11 ± 1.05*
24	76.604 ± 1.225	0.142 ± 0.011	539	10.739 ± 0.10	58.217 ± 1.407	5	—
25	*28.154 ± 1.093*	**0.066** ± 0.004	*426*	*0.835 ± 0.10*	*14.130 ± 0.639*	*17*	*14.08 ± 0.24*
26	*19.881 ± 1.172*	*0.327 ± 0.011*	*60*	*0.890 ± 0.10*	*1.034 ± 0.031*	*1*	*19.52 ± 0.18*
27	na	30.181 ± 1.183	—	49.033 ± 0.10	na	—	—
28	*10.094 ± 0.239*	**0.219 ± 0.34**	*46*	*1.482 ± 0.10*	*9.251 ± 0.506*	*6*	*11.29 ± 0.08*
29	21.428 ± 0.316	0.395 ± 0.34	54	3.642 ± 0.10	34.043 ± 1.18	9	—
Safinamide	8.204 ± 0.195	0.030 ± 0.001	273	—	—	—	—
Donepezil	—	—	—	0.055 ± 0.011	6.283 ± 0.026	114	—
Curcumin	—	—	—	—	—	—	7.29 ± 0.03

[a] Values represent mean ± SEM; $n = 3$. [b] Selectivity index = SI = IC_{50} of MAO-A/IC_{50} of MAO-B and IC_{50} of BChE/IC_{50} of AChE; bold and italics boxes represents the compounds that have balanced (moderate to excellent) biological activities against all tested targets. na = no activity found in the tested concentration.

using tyramine as a nonselective substrate of these two human isoforms. Furthermore, linear-type of compounds like safinamide are considered suitable for MAO-B inhibition. Our designed compounds in *trans*-isomeric form showed linearity. Hence, the synthesized FA derivatives are anticipated to show selectivity towards MAO-B. The results presented in Table 2 showed that compounds, except GA derivative **27**, exhibited inhibition potential towards MAO-B in submicromolar to nanomolar concentration. All the synthesized derivatives exhibited high selectivity towards MAO-B. 6-Hydroxy benzothiazole-biphenyl hybrid (cinnamic acid derivative **23**) emerged as the most potent MAO-B inhibitor with IC_{50} value of 0.037 μM that might be due the linearity in structure, 6-hydroxy benzothiazole moiety and the bi-phenyl cinnamic acid having hydrophobic regions. Moreover, the benzyloxy FA derivative containing alaninamide moiety (**19**) showed IC_{50} value of 0.318 μM (SI = 281). While FA analogue **18** showed moderate MAO-B inhibition. Another analogue with benzyloxy and sulfonamide moiety showed excellent activity with IC_{50} value of 0.066 μM. GA derivative with 6-hydroxy benzothiazole also displayed excellent activity towards MAO-B with IC_{50} value of 0.219 μM (SI = 281). Overall, modification on FA at R as benzyloxy group (**19**, **22** and **25**) achieved more significant hMAO-B inhibition.

Self-mediated $A\beta_{1-42}$ aggregation inhibition

In order to evaluate the effects of substances on $A\beta_{1-42}$ aggregation, the $A\beta_{1-42}$ peptide was exposed to each compound at 1.5 equivalent concentrations (1 : 0.5 and 1 : 1). The $A\beta_{1-42}$ peptide's tendency to aggregate was examined using the Thioflavin T-fluorescence (ThT) test. ThT, a fluorescent dye that selectively binds to fibrous structures, allowed us to determine the progression of $A\beta_{1-42}$ aggregation over time in the presence of selected compounds (**23**, **25** and **28**). The samples treated with curcumin (standard drug/positive control) and synthesized derivatives showed reduced fluorescence intensity in comparison to a control sample that included only the $A\beta_{1-42}$ peptide. More specifically, there was less production of amyloid fibrils in the samples treated with curcumin, compounds **23**, **25**, and **28**. Remarkably, compound **28** treated sample showed, at least partially, less aggregation than compound **23** and compound **25**. Curcumin and compound **28** showed around 60% inhibition of amyloid beta fibrils after a 24-hour equimolar administration, but compound **23** and compound **25** showed approximately 30% and 50% inhibition, respectively (Fig. 4).

Overall, we were successful in synthesizing compounds **23**, **25**, **26** and **28** (yellow highlighted cells in Table 2) that have balanced (moderate to excellent) biological activities against all tested targets.

The investigation spanned 48 hours and involved different doses. Notably, our findings, as illustrated in Fig. 5a and b, revealed that even at the maximum concentration of 100 μM, compounds **23**, **25**, **28**, and **29** did not show any apparent neurotoxicity. However, compound **27** has shown 40–50% protective ability at all concentrations on human neuroblastoma cell line (SH-SY5Y) as compared to other compounds as well as trolox. Furthermore, reference compounds donepezil, rasigiline, and trolox exhibited no cytotoxicity at any of the tested concentrations. These compelling results suggest that compounds **23**, **25**, **28**, and **29** hold promise as effective multifunctional agents in the management of AD, opening new avenues for potential therapeutic interventions.

Concentration-dependent self-mediated $A\beta_{1-42}$ aggregation inhibition

Subsequently, a study on concentration-dependent self-mediated suppression of $A\beta_{1-42}$ aggregation was carried out. $A\beta_{1-42}$ was subjected to incubation with or without different doses of the synthesized compounds at different concentrations in μM. Table 2 provides results of self-mediated $A\beta_{1-42}$ aggregation inhibition (IC_{50} values in μM). Compounds **28** and **25** (IC_{50} values of 11.29 μM, and 14.08 μM, respectively) showed moderate results in blocking self-mediated $A\beta_{1-42}$ aggregation. Furthermore, curcumin, the reference compound, showed an IC_{50} value of 7.29 μM. Dose response curves were then determined using the ThT assay for the two best inhibitors **23** and **28** as indicated by the ThT assay. For each inhibitor, a dose response was obtained over at least 5 concentrations and an IC_{50} was determined using GraphPad PRISM (Fig. S-7 in ESI†). Curcumin (IC_{50} 7.29 ± 0.03 μM), compound **28** (IC_{50} 11.29 ± 0.08 μM) and compound **23** (IC_{50} of 23.11 ± 1.05 μM). IC_{50} values are the average of 3 independent determinations.

Inhibition of COX-2 and 5-LOX

The AD patient has elevated levels of cyclooxygenase-2 (COX-2) and 5-lipoxygenase (5-LOX) in the brain which results in neuro-inflammation, specifically in case of in 5-LOX expression it has been linked to elevated Aβ production. Inhibition of 5-LOX and COX-2 can delay the onset and/or slow down the course of age-related brain disorders.[3,15] *In vitro* inhibition assays against COX-2 and 5-LOX were performed for the selected compounds (**23**, **25**, **26**, and **28**). Celecoxib for COX-2 and Zileuton for 5-LOX were used as reference drug in assays. The results of inhibition (IC_{50} in μM) in are presented in

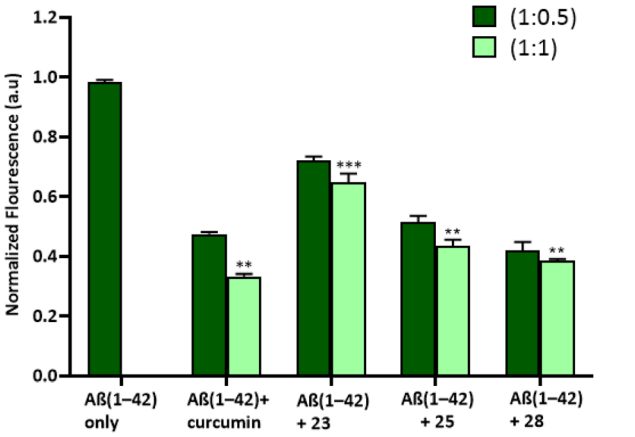

Fig. 4 Bar diagram illustration of the effect of curcumin and compounds (**23**, **25**, and **28**) on ThT fluorescence and aggregation of $A\beta_{(1-42)}$ peptide after incubated for 24 hours. *P < 0.05, **P < 0.01 and ***P < 0.001.

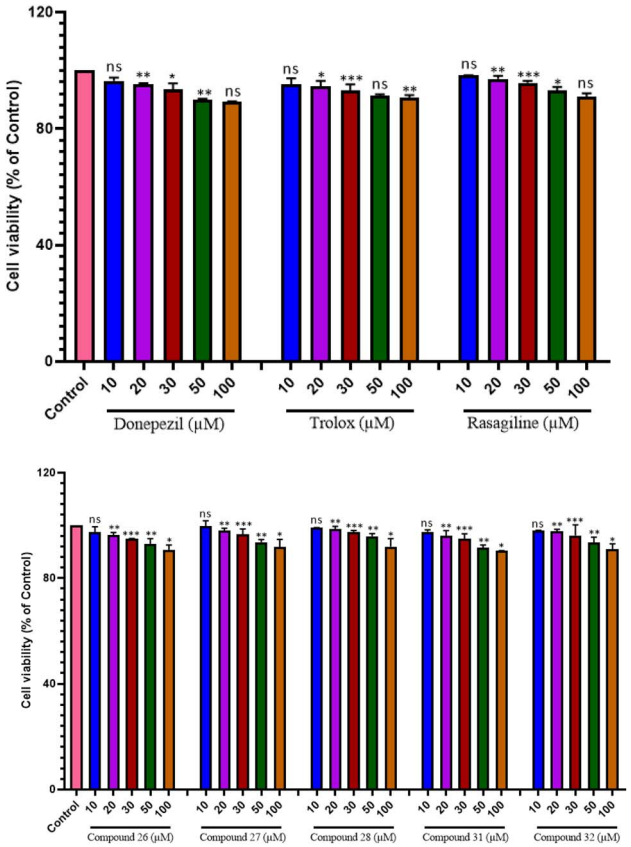

Fig. 5 Cytoprotective and cytotoxic effect of compounds on SH-SY5Y cells. Cytotoxic activity after 48 h incubation with compounds **23**, **25**, **27**, **28**, **29** and donepezil, trolox, rasagiline at 10 μM, 20 μM, 30 μM, 50 μM and 100 μM on SH-SY5Y cells. *P < 0.05, **P < 0.01, ***P < 0.001 and ns = non-significant.

Table 3. Selected compounds *in vitro* results exhibited that compound **25** containing sulfonamide moiety and amide linkage showed better inhibition results having IC_{50} = 0.74 ± 0.13 μM for COX-2. Other selected compounds (**23**, **26** and **28**) also showed moderate results in sub-micromolar range having IC_{50} = 14.38, 2.19 and 10.44 μM respectively (Table 3). Compound **28** containing GA, benzothiazole and having amide linkage between them have exhibited most potent inhibition results having IC_{50} = 0.47 ± 0.04 μM for 5-LOX which is better result as compared to reference drug (zileuton) used in assay. Other selected compounds (**23**, **25** and **26**) also exhibited comparable inhibition results in sub-micromolar range having IC_{50} = 0.59, 5.96 and 1.17 μM respectively (Table 3).

SH-SY5Y neuroblastoma cell toxicity

The pursuit for safe medications that influence the central nervous system (CNS) is crucial. In our pursuit of this goal, we subjected potent inhibitors to rigorous cytotoxicity testing using the human neuroblastoma cell line (SH-SY5Y) to evaluate the biological safety of these compounds.[3,56,59] We conducted a study examining the cytotoxic effects of selected compounds **23**, **25** and **27–29**, along with reference compounds donepezil, trolox, and rasagiline, on the human neuroblastoma cell line SH-SY5Y.

Table 3 *In vitro* inhibition results of COX-2 and 5-LOX

	IC_{50} (μM) ± SEM[a]	
Entry	COX-2	5-LOX
23	14.38 ± 0.28	0.59 ± 0.08
25	0.74 ± 0.13	5.96 ± 0.19
26	2.19 ± 0.10	1.17 ± 0.07
28	10.44 ± 0.13	0.47 ± 0.04
Celecoxib	0.05 ± 0.01	—
Zileuton	—	0.575 ± 0.11

[a] Values represent mean ± SEM; n = 3

Neuroprotective effect on H_2O_2-induced oxidative toxicity in SH-SY5Y cells

The aberrant metabolic oxidation events, such as the generation of hydroxyl radical (OH•) and hydrogen peroxide (H_2O_2), within the central nervous system, leading to oxidative stress, are believed to be significant factors in the development of AD. In recent years, strategies aimed at scavenging free radicals and preventing the overproduction of reactive oxygen species (ROS) have gained attraction as potent approaches for both the treatment and prevention of AD. To assess their protective properties against free radical damage, compounds **23**, **25**, **28**, and **29** were specifically selected and their ability to counteract H_2O_2 harm was evaluated. Trolox was used as the reference compound.

Cell viability was represented as a percentage, with the control group set at 100%. As shown in Fig. 6 notably, compounds **23**, **25**, **28** and **29** exhibited striking protective results at 50 μM concentration when exposed to H_2O_2 (400 μM). Compounds **25** and **23** having 81.40% and 80.4% showed the most potent neuroprotective activity. While compound **29**

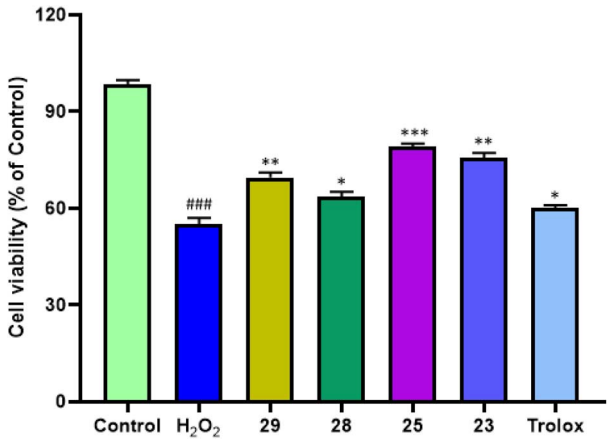

Fig. 6 Cytoprotective effects of compounds **23**, **25**, **28** and **29** against H_2O_2-induced cell death on SH-SY5Y cells. Cell viability was measured by MTT assay and data were expressed as a percentage of viable cells (referred to control). Data is expressed as mean ± SD of three assays. ###P < 0.001 *vs.* the control group, *P < 0.05 *vs.* the H_2O_2 group treated with of H_2O_2 (400 μM) while **P < 0.01 and ***P < 0.001.

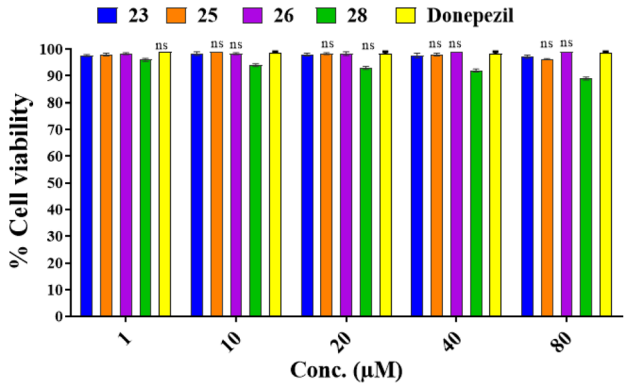

Fig. 7 Cell viability assay results of compounds **23**, **25**, **26**, and **28** on normal human embryonic HEK-293 cells model at 1, 10, 20, 40 and 100 μM concentrations as obtained from MTT assays. Two-way ANOVA and the Bonferroni test were followed. Data were represented as mean ± S.E.M.; all the values were not-significant (ns) to that of the control group.

Table 4 *In vitro* PAMPA-BBB penetration results

Compounds label	Permeability (PAMPA-BBB)[a] $P_{e(tested)}$ (10^{-6} cm s^{-1})	Prediction of CNS penetration
23	5.9	High
25	6.4	High
27[b]	*0.01*	*No*
28	5.0	High
29	*0.37*	*No*
Donepezil	16.7	High
Validation of the model by seven commercial drugs		
Diazepam	15.30	High
Atenolol	0.75	No
Alprazolam	5.60	High
Lomefloxacin	1.12	No

[a] Data represent are the assay mean for the marketed drugs ($n = 3$). b'CNS+' (prediction of high BBB permeation); Pe (10^{-6} cm s^{-1}) > 4.39. c'CNS−' (prediction of low BBB permeation); Pe (10^{-6} cm s^{-1}) < 1.78. [b] Italics cells showed compounds with no BBB permeability.

(70.6%) and **28** (63.5%) exhibited the least neuroprotective activity that was also better than trolox (62.8%). The structural features of the most potent compound, particularly the increased presence of aromatic rings (electron-rich species) in compounds **25** and **23**, represent a significant divergence from other compounds. This heightened aromaticity may potentially contribute to enhanced radical scavenging effects, thereby leading to a more pronounced neuroprotective impact overall.

Cell viability assay on normal human embryonic HEK-293 cells model

MTT assay was utilized in order to evaluate the selected compounds (**23**, **25**, **26**, and **28**) on HEK-293 cells (human embryonic cells) for their cytotoxicity potential. The results of these studies revealed that all the compounds have not showed in cytotoxic effect on the viability of normal cells, which means they are safe for non-cancerous cells. The results of this assay are presented in Fig. 7.

PAMPA BBB assay

Based on antioxidant and enzyme inhibition activity, we selected compounds **23**, **25**, **27–29** for a parallel artificial membrane permeation assay (PAMPA).[15,60,61] FA derivatives **23** and **25** showed BBB high penetration. However, among GA derivatives only 28 showed high permeability (Table 4). Compounds **27** and **29** were found to be CNS negative in the *in vitro* PAMPA experiment.

In vivo anti-oxidant assays

Effects of synthesized compounds on SOD, GHS-Px, MDA and CAT activity. Oxidative stress has been associated with memory deficit. Due to higher consumption of oxygen and metabolic activity, our brain is more susceptible ROS induced neurotoxicity. In current study, compounds **23**, **25**, **28** and **29** were tested for their *in vivo* antioxidant potential (superoxide dismutase, catalase and GSH). The results have been presented as graph in Fig. 8a–d. Results showed that all the selected compounds, except **29**, cause a significant free-radical scavenging activities by decreasing SOD, CAT and GSH activities.

Superoxide dismutase, catalase and glutathione peroxide are group of enzymes that play vital or protective role in providing first line antioxidant defense to the biological systems against ROS. Superoxide dismutase (SOD) catalyse the conversion superoxide to hydrogen peroxide and hydrogen. With the increase in free radical formation/age, the levels of SODs decrease.

Superoxide dismutase (SOD) levels were observed to be 36.50 U mL^{-1} in animal brains. This level is significantly lower compared with the control group (Fig. 8a). However, trolox (positive control) and compound **28** have shown significant antioxidant potential. This was observed by an increase in SOD level as compared to the model group. During the treatment with compound **28** (5 mg), 94.20 U mL^{-1} protein was observed in the brain's SOD level.

Similarly, the brain's GSH-Px activity was 240 U per mg protein, showing that the ageing model groups had lower GSH-Px levels than other groups. As a consequence, treatment with compound **28** increases the antioxidant enzymatic activity of GSH-Px (Fig. 8b).

In control groups of the ageing model the malondialdehyde (MDA) levels were observed to be considerably greater (Fig. 8c). Treatment with compound **28** (5 mg) resulted in less MDA concentration of animals (1.15 nmol mL^{-1}) in animal brains that was particularly lesser than other groups. The high-test dose was 97 U mL^{-1} during the CAT activity as shown in Fig. 8d, which was notably higher than other treated groups. It demonstrates there is a notable impact on CAT activities due to strain concentration. The results show that the treated mice brain has increased CAT activity that is might due to compound **28**. Overall, other compounds, such as **23** and **28**, had good to moderate *in vivo* antioxidant activity. Compound **29** was the only one not determined to be active when compared to the others since it did not penetrate the BBB.

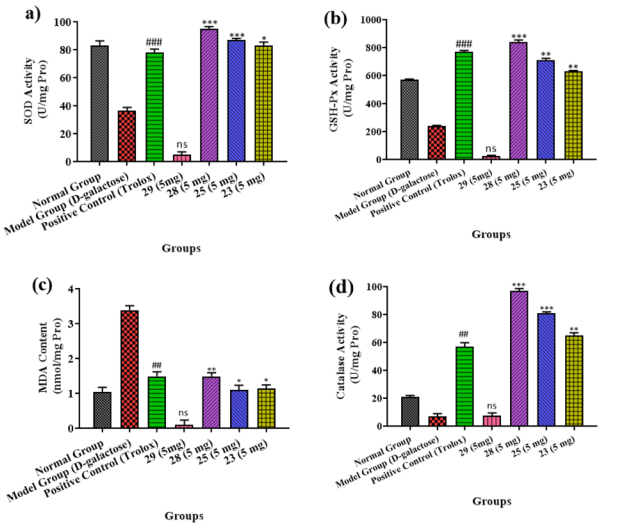

Fig. 8 (a–d) SOD, GSH-Px, MDA and CAT activity in the brain of mice across various treatment groups. Distinct lowercase letters denote a significant difference in SOD, GSH-Px, MDA & CAT activity within the same organ among treatment groups. The data is shown as mean ± S.E.M; significant differences in values from the positive control; $n = 3$, ##$P < 0.01$ *vs.* the control group, ns; non-significant * = $P < 0.05$, ** = $P < 0.01$, *** = $P < 0.001$ to that of the positive control.

Docking studies

To evaluate the binding affinities and profile of inhibition of the compounds with the targets including MAO-B and AChE, molecular docking analysis was executed by using the program Molecular Operating Environment (MOE). The co-crystal ligands were docked in-to the active sites of the targets to validate the docking investigations. The compounds' docking poses display conformations that are similar to their co-crystal confirmations. This indicates that an efficient docking procedure was applied. The crystallographic structure of targets was retrieved from the Protein Data Bank base in the PDB format with PDB accession codes 1EVE for AChE and 2V5Z for MAO-B.

Active site constitution of MAO-A and MAO-B

The structure of MAO-A (hMAO-A) has two domains in its structure including the extra membrane and membrane binding domain. The future division of the extra membrane domain is such that it consists of an FAD-binding region and an inhibitor-binding region. The active site region of the hMAO-A has 550 Å volume. The key residues for the MAO-A inhibition include Tyr444, Tyr407, Phe352, Leu337, Ile335, Ile335, Cys323, Gln215, Val210, Phe208, Asn181, and Tyr69. While on the other hand similar to the MAO-A the MAO-B also have two domains, extra membrane and membrane binding domain. The extra membrane binding domain has two regions, also named as FAD and inhibitor/substrate binding region. The hMAO-B binding site consists of two regions, the entrance cavity having approximately 290 Å volume and the inhibitor binding site (flat hydrophobic site) having approximately 420 Å volume. The key residues in the entrance cavity include Tyr326, Ile316, Ile199, Leu171, Phe168, Leu167, Leu164, Trp119, Pro104, and Phe103. The gateway between the two cavities is from the entrance cavity region residue (Ile199). The C-terminal (substrate bind site) include Tyr435, Tyr398, Tyr326, Gln206, Ile198, Leu171, Cys172, Tyr60, Ser59 and Tyr60 amino acid residues.

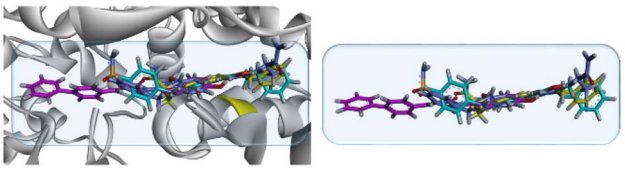

Fig. 9 3D modelled diagram of compounds **19**, **23**, **25** superposed on co-crystallized ligand safinamide (yellow) in the binding site of MAO-B (2V5Z).

Our designed compounds in *trans*-isomeric form showed linearity in their most stable/lowest energy conformation. The superposed diagram of **19**, **23** and **25** on safinamide is shown in Fig. 9.

Binding mode of 23, 26, and 28 in binding site to MAO-A

The visual inspection of the binding mode of **23** in the binding site of MAO-A revealed hydrophobic binding affinities through both aromatic terminal regions of the molecules (benzothiazole and bi-phenyl region), including Cys323 and Cys406 having π–sulfur interaction (Fig. 10a). In contrast, other interactions include Phe208 (π–sigma), Tyr407, and Tyr444 (π–π T-shaped) binding affinities. Furthermore, a binding inspection of compound **26** revealed that hydrophilic (hydrogen bond) binding affinity was exhibited by Ala111, other hydrophobic binding affinities include Cys406 (π–sulfur), Tyr407 (π–π stacked) and Phe208 (π–sigma) (Fig. 10b). Compound **28** visual inspection in the binding site also revealed that the OH moieties present in the structure of gallic acid had formed three hydrophilic conventional hydrogen bonds with the binding site residues including Phe208, Gln215, and Thr336. While it only displayed one hydrophobic π–sulfur interaction with Tyr69 (Fig. 10c).

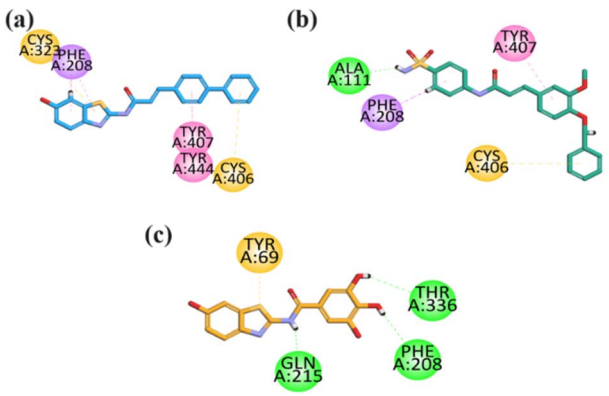

Fig. 10 2D interaction plot of compound (a–c) **23**, **26**, **28** in the binding site of MAO-A (2Z5X) modelled by using Discovery Studio visualizer.

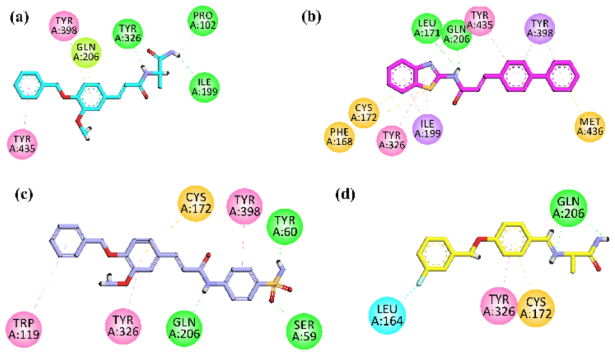

Fig. 11 2D interaction plot of compounds (a–c) **19**, **23**, **25** and (d) safinamide in the binding site of MAO-B (2V5Z), modelled by using Discovery Studio visualizer.

Binding mode of 19 in the binding site of MAO-B

The visual inspection of the binding mode of **19** in the binding site of MAO-B revealed that amine regions at the terminal side is towards the gateway region, it displayed hydrophilic interactions with the Pro102 and Ile199 (gateway residue between two cavities of MAO-B binding site). The aromatic region of the **19** has oriented itself to the C-terminal (substrate binding site) of the active site by interacting with the Tyr398, Tyr435, and Gln206 by hydrophobic (π–π and π–lone) interactions, Tyr326 exhibited hydrophilic interaction with the amine region near to aromatic region (Fig. 11a). These visual inspection result of compound **19** revealed that mimic the alanine portion of the safinamide at one terminal end, aromatic region on the other end of molecule might have played vital rule in good inhibition results of MAO-B.

Binding mode of 23 in the binding site of MAO-B

Analysis of the most potent compound **23** having biphenyl and benzothiazole moieties revealed that it has oriented itself completely by covering the substrate binding residues and only the gateway residue Ile199. Benzothiazole moiety oriented itself near the gateway region by forming the π–σ interaction with Ile199, from there it also exhibited hydrophobic interactions with Cys172, Phe168 (π–sulfur), Tyr326 (π–alkyl), and its amine region attached to bi-phenyl in the mid-region displayed hydrophilic interaction with Gln206 and Leu171 (hydrogen bond). While the other part of the compound (biphenyl region) oriented itself to the inner side by interacting hydrophobically with Tyr398 (π–sigma), Tyr435 (π–π) and Met436 (π–sulfur) (Fig. 11b). These visual inspection result of compound **23** revealed that the benzothiazole, amide region, the bi-phenyl region and linearity in structure might have played role in MAO-B inhibition.

Binding mode of 25 in the binding site of MAO-B

The visual inspection of sulfonamides derivative **25** in the binding site of the receptor revealed that its sulfonamide group oriented itself in the substrate binding site by interacting with hydrophilicity (hydrogen bond interaction) with the residue Gln206, Ser59, and hydrophobically with the Tyr398. Moreover, the aromatic region of **25** binds hydrophobically with the Cys172 (π–sulfur), Tyr326 (π–π), and Trp119 (π–π) (Fig. 11c). These visual inspection result of compound **25** revealed that with aromatic region, amide linkage and especially in this case benzene sulfonamide moiety might have played role in the inhibition potential.

Binding mode of standard drug safinamide in the binding site of MAO-B

The co-crystalized ligand safinamide was also visually inspected in the binding site of MAO-B, it oriented itself in the substrate binding site by hydrophobic interaction with residues including Tyr326 (π–π), Cys172 (π–sulfur) and its (amine region) also exhibited hydrophobic interaction with Gln206 (hydrogen bond interaction). Its terminal aromatic region having F group forms halogen interaction with leu164 (Fig. 11d).

Binding mode of 23 in the binding site of AChE

The active site of AChE containing key residues that are vital for inhibition includes Trp84, Glu199, Phe330 (CAS region), Trp279, Tyr70, Asp72 (PAS region) and Gly118, Gly119 Ala201, Trp233, Phe288, Phe290, Phe331 (mid gorge region). The binding affinities of the most potent compound **23** exhibited similar interactions to donepezil, including π–π interactions with Trp84, His440, and Phe331 with the benzothiazoles aromatic region of the compound. While the other terminal side of a molecule having bi-phenyl aromatic regions displayed π–π hydrophobic binding affinities with the Trp279, Tyr70, and Tyr334. The carbonyl oxygen of the compound displayed hydrophilic hydrogen bond interactions with Ser122 and Tyr121 (Fig. 12). These visual inspection results of compound **23** in the pocket of AChE revealed that benzothiazole aromatic region, an aromatic region on the other terminal of the molecule might have enabled the molecule to exhibit the most potent inhibition results among the synthesized compounds. Literature studies revealed that the interaction of compounds with Trp84 and Trp279 (also termed as dual binding site inhibitors) resulted in high AChE inhibition potential.[3] The high activity of compound 23 may be due to its hydrophobic regions on both terminals (benzothiazole and cinnamic acid). Standard drug donepezil also interacts with Trp84 and Trp279 (Fig. S-8 ESI†).

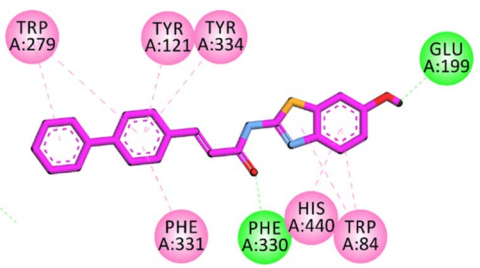

Fig. 12 2D interaction plot of compound **23** in the binding site of AChE (1EVE), modelled by using Discovery Studio visualizer.

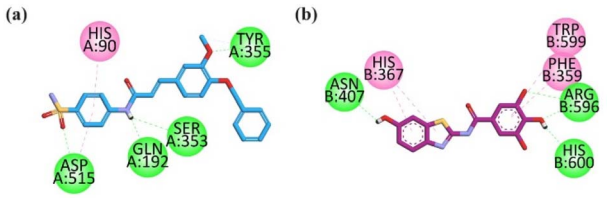

Fig. 13 2D interaction plot of compound **25a** in the binding site of (a) compound **25** in the binding site of COX-2 (1CX2), and (b) compound **28** in binding site of 5-LOX (6N2W) modelled by using Discovery Studio visualizer.

Binding mode of 25 in the active site of COX-2

Most potent compound **25** was docked into the active site of COX-2 (PBD ID = 1CX2) having S58 (selective inhibitor), to find the binding affinities by using a molecular modelling study. The selective inhibitor (native ligand) of COX-2 displayed binding affinities with important residues including hydrophilic binding affinities with COX-2 specificity pocket residue (Arg513, Asp515, Leu352, Ser353 and His90), Tyr355, Arg120 and hydrophobic interactions with Val349, Val523, Tyr385, and Trp387. Visual inspection of compound **25** revealed that benzene sulfonamide moiety oriented itself towards the COX-2 specificity pocket and formed 3 hydrophilic hydrogen bond interactions with Asp515, Gln192 and Ser353 and a π–π binding affinity with His90. While $-OCH_3$ formed an H-bond with Tyr355 (Fig. 13a). Sulfonamide is considered an important core to favour COX-2 potency. All marketed COX-2 drugs except lumiracoxib contain sulfonamide moiety. The standard drug celecoxib (nanomolar inhibitor) also oriented itself deep in the specific pocket (Fig. S-9 in ESI†). These binding results of compound **23** due to the benzene sulfonamide might have played vital role in inhibition results of COX-2. The computed binding free energy values for compound **25** in the pocket of COX-2 is -8.9768 kcal mol^{-1}.

Binding mode of 28 in the active site of 5-LOX

The docking analysis of compound **28** in the binding site of 5-lipoxygenase (5-LOX) to figure out the binding affinities and interaction with amino acid residues. The co-crystallized structure of 5-lipoxygenase (6N2W) with nordihydroguaiaretic acid (NDGA) was selected for docking analysis. NDGA showed binding affinities with important residues including His600, Asn407, Leu607, Trp599, Arg596, Phe359, His372, and Ala410. Visual inspection in the pocket revealed that compound **28** oriented itself in the pocket of 5-LOX such that the –OH groups attached to the GA at one end of the molecule forms H-bonds (hydrophilic binding affinity) with important residues including His600 and Arg596. The hydrophobic region of GA showed binding orientation with Trp599 and Phe359. Furthermore, the benzothiazole –OH group oriented itself towards the important residue Asn407 (hydrophilic H-bond) and the hydrophobic region of benzothiazole exhibited π–π binding orientation with His 367 (Fig. 13b). The binding free energy score for compound 28 in the 5-LOX pocket is -7.658 kcal mol^{-1}. This visual inspection of compound **28** revealed that the benzothiazole moiety having –OH and GA having –OH groups might have played an important role in good inhibition results.

Conclusions

Reactive oxygen species (ROS) generation is known to be significantly influenced by types A and B of monoamine oxidases (MAOs), which catalyse the metabolic oxidation of monoamine neurotransmitters. Monoamine oxidases (MAOs) inhibitors could decrease reactive oxygen species (ROS) generation (oxidative-stress), enhance mono-aminergic neural transmission, and have major therapeutic benefits which could be useful in case of A. In current research, we focused to develop multitarget framework for oxidative stress related AD therapy. Antioxidant properties of synthesized derivatives of sulfonamide, alanine and 2-aminobenzothiazole in conjunction of bioactive portion containing ferulic acid (FA)/gallic acid (GA) have also been explored. The results of DPPH and ABTS radical scavenging assay indicated that GA derivatives **27–29** have excellent abilities to scavenge free radicals. FA analog **23** with biphenyl group and 6-hydroxybenzothiazole core relatively emerged as an excellent antioxidant with FRAP value of 53.57 μM. Whereas, benzyloxy- and biphenyl-containing amides (**19** and **20**) also showed good antioxidant activity. The inclusion of anelectron-withdrawing SO_2NH_2 resulted in low antioxidant activity. Compound **28** with GA (three hydroxyl groups) and 6-hydroxybenzothiazole core also emerged as excellent antioxidant with FRAP value of 45.24 μM. In MAO-B and AChE inhibition assay results, 6-hydroxy benzothiazole-biphenyl hybrid (cinnamic acid derivative **23**) emerged as the most potent MAO-B inhibitor with IC_{50} value of 0.037 μM and 0.071 μM, respectively. Furthermore, the AD patient has elevated levels of cyclooxygenase-2 (COX-2) and 5-lipoxygenase (5-LOX) in the brain which results in neuro-inflammation, specifically in case of in 5-LOX expression it has been linked to elevated Aβ production. Inhibition of 5-LOX and COX-2 can delay the onset and/or slow down the course of age-related brain disorders. The *in vitro* COX-2 and 5-LOX inhibition results showed that the selected compounds exhibited IC_{50} value in low micromolar concentration to submicromolar level. Literature studies revealed that Aβ and oxidative stress (OS) are interlinked as Aβ can induce OS resulting in an increase in Aβ deposition. Selected compounds **23**, **25**, **26** and **28** displayed good to moderate inhibition of self-mediated amyloid β_{1-42} peptide aggregation in ThT assay. Moreover, selected compounds showed nearly no neurotoxicity on SH-SY5Y cells and also showed excel-lent neuroprotective effect against H_2O_2-induced SH-SY5Y cells. Brain antioxidant enzymes superoxide dismutase (SOD), catalase, and glutathione peroxidase (GSH-Px) were studied in the brain of male BALB/c mice. All the tested compounds except **29** have shown good to moderate ex-vivo antioxidant potential. In short, the findings of the current study are promising for further development of LEAD compounds to combat neurodegenerative diseases like AD.

Ethical statement

We followed the Ethical Guidelines for Animal Testing. The Ethical Committee of the Department of Pharmacy at Bacha Khan University, Pakistan *via* departmental ethical committee number (DECN/-2023–05) approved all the protocols. All the *in vivo* experiments were conducted in accordance with the Animals Bye – Laws of 2008 (Scientific Procedure, Issue-I).

Author contributions

UR conceived, designed, and supervised this study. He was involved in all the phases (from synthesis to pharmacological evaluation and manuscript writing/editing) that led to the completion of the manuscript. FH and AT synthesized the compounds. *In vitro* experiments were performed by FH, AT and AS. Docking studies were performed FH and NF. Docking results were analysed and written by UR. MSJ performed *in vivo* studies. Manuscript was drafted by FH and UR. UR reviewed and edited the drafts. All the authors have read the manuscript and approved it for publication. The authors declare that there is no conflict of interest.

Conflicts of interest

The authors declare no conflict of interest.

Acknowledgements

The research is financially supported by Project Grant from the Higher Education Commission Pakistan to Umer Rashid (PI) under National Research Program for Universities (NRPU) (20-14513/NRPU/R&D/HEC/2021 2021).

References

1 U. Rashid and F. L. Ansari, in *Drug Design and Discovery in Alzheimer's Disease*, Elsevier, 2014, pp. 40–141.
2 J. Xu, S. Patassini, P. Begley, S. Church, H. J. Waldvogel, R. L. Faull, R. D. Unwin and G. J. Cooper, *Biochem. Biophys. Res. Commun.*, 2020, **527**, 676–681.
3 M. A. Javed, N. Ashraf, M. Saeed Jan, M. H. Mahnashi, Y. S. Alqahtani, B. A. Alyami, A. O. Alqarni, Y. I. Asiri, M. Ikram and A. Sadiq, *ACS Chem. Neurosci.*, 2021, **12**, 4123–4143.
4 M. Zvěřová, *Clin. Biochem.*, 2019, **72**, 3–6.
5 F. J. Vajda, *J. Clin. Neurosci.*, 2002, **9**, 4–8.
6 A.-C. S. Vogt, G. T. Jennings, M. O. Mohsen, M. Vogel and M. F. Bachmann, *Int. J. Mol. Sci.*, 2023, **24**, 3895.
7 R. Sengoku, *Neuropathology*, 2020, **40**, 22–29.
8 L. Fan, C. Mao, X. Hu, S. Zhang, Z. Yang, Z. Hu, H. Sun, Y. Fan, Y. Dong and J. Yang, *Front. Neurol.*, 2020, **10**, 1312.
9 E. Karran and B. De Strooper, *Nat. Rev. Drug Discovery*, 2022, **21**, 306–318.
10 D. Padhi and T. Govindaraju, *J. Med. Chem.*, 2022, **65**, 7088–7105.
11 A. Porsteinsson, R. Isaacson, S. Knox, M. Sabbagh and I. Rubino, *J. Prev. Alzheimers Dis.*, 2021, **8**, 371–386.
12 Y. P. Singh, H. Rai, G. Singh, G. K. Singh, S. Mishra, S. Kumar, S. Srikrishna and G. Modi, *Eur. J. Med. Chem.*, 2021, **215**, 113278.
13 Z. Ozdemir, A. Ozcelik and M. Uysal, *Frontiers in Clinical Drug Research-Alzheimer Disorders*, 2019, vol. 8, pp. 154–190.
14 S. Lista, A. Vergallo, S. J. Teipel, P. Lemercier, F. S. Giorgi, A. Gabelle, F. Garaci, N. B. Mercuri, C. Babiloni and B. P. Gaire, *Ageing Res. Rev.*, 2023, **84**, 101819.
15 M. A. Javed, S. Bibi, M. S. Jan, M. Ikram, A. Zaidi, U. Farooq, A. Sadiq and U. Rashid, *RSC Adv.*, 2022, **12**, 22503–22517.
16 D. G. Wilkinson, P. T. Francis, E. Schwam and J. Payne-Parrish, *Drugs Aging*, 2004, **21**, 453–478.
17 R. N. Rosenberg, D. Lambracht-Washington, G. Yu and W. Xia, *JAMA Neurol.*, 2016, **73**, 867–874.
18 O. M. Waly, K. M. Saad, H. I. El-Subbagh, S. M. Bayomi and M. A. Ghaly, *Eur. J. Med. Chem.*, 2022, **231**, 114152.
19 A. H. Hassan, H. J. Kim, K. Park, Y. Choi, S. Moon, C. H. Lee, Y. J. Kim, S. B. Cho, M. S. Gee and D. Lee, *Antioxidants*, 2023, **12**, 1033.
20 A. Elkamhawy, J. Woo, N. A. Gouda, J. Kim, H. Nada, E. J. Roh, K. D. Park, J. Cho and K. Lee, *Antioxidants*, 2021, **10**, 1604.
21 M. Naoi, W. Maruyama and M. Shamoto-Nagai, *Int. J. Mol. Sci.*, 2022, **23**, 11059.
22 T. Behl, D. Kaur, A. Sehgal, S. Singh, N. Sharma, G. Zengin, F. L. Andronie-Cioara, M. M. Toma, S. Bungau and A. G. Bumbu, *Molecules*, 2021, **26**, 3724.
23 S. Manzoor and N. Hoda, *Eur. J. Med. Chem.*, 2020, **206**, 112787.
24 R. Jadoon, M. A. Javed, M. S. Jan, M. Ikram, M. H. Mahnashi, A. Sadiq, M. Shahid and U. Rashid, *Bioorg. Med. Chem. Lett.*, 2022, **76**, 128994.
25 I. T. Lott and E. Head, *Nat. Rev. Neurol.*, 2019, **15**, 135–147.
26 E. Tamagno, M. Guglielmotto, V. Vasciaveo and M. Tabaton, *Antioxidants*, 2021, **10**, 1479.
27 H. Turkez, M. E. Arslan, J. N. Barboza, C. Y. Kahraman, D. P. de Sousa and A. Mardinoğlu, *Curr. Drug Delivery*, 2022, **19**, 860–873.
28 J.-S. Lan, R.-F. Zeng, X.-Y. Jiang, J.-W. Hou, Y. Liu, Z.-H. Hu, H.-X. Li, Y. Li, S.-S. Xie and Y. Ding, *Bioorg. Chem.*, 2020, **94**, 103413.
29 S. Shabani, Z. Rabiei and H. Amini-Khoei, *Int. J. Food Prop.*, 2020, **23**, 736–752.
30 X. F. Huang, Z. An, Y. C. Yu, X. Q. Feng and Y. J. Wang, *ChemistrySelect*, 2022, **7**, e202200650.
31 K. I. Eissa, M. M. Kamel, L. W. Mohamed, A. S. Doghish, R. Alnajjar, A. A. Al-Karmalawy and A. E. Kassab, *Drug Dev. Res.*, 2023, **84**, 937–961.
32 W. Sun and M. H. Shahrajabian, *Molecules*, 2023, **28**, 1845.
33 J. Gao, J. Hu, D. Hu and X. Yang, *Nat. Prod. Commun.*, 2019, **14**, 1934578X19874174.
34 M. Xu, P. Meng, H. Wang, J. Liu, T. Guo, Z. Zhu and Y. Bi, *Antioxidants*, 2023, **12**, 1473.

35 Z. Zhang, J. Guo, M. Cheng, W. Zhou, Y. Wan, R. Wang, Y. Fang, Y. Jin, J. Liu and S.-S. Xie, *Eur. J. Med. Chem.*, 2021, **213**, 113154.
36 Y.-W. Tang, C.-J. Shi, H.-L. Yang, P. Cai, Q.-H. Liu, X.-L. Yang, L.-Y. Kong and X.-B. Wang, *Eur. J. Med. Chem.*, 2019, **163**, 307–319.
37 M. S. Jan, S. Ahmad, F. Hussain, A. Ahmad, F. Mahmood, U. Rashid, F. Ullah, M. Ayaz and A. Sadiq, *Eur. J. Med. Chem.*, 2020, **186**, 111863.
38 Z. Mao, Y.-L. Zheng and Y.-Q. Zhang, *Int. J. Mol. Sci.*, 2010, **12**, 114–127.
39 H. Kuthan, H.-J. Haussmann and J. Werringloer, *Biochem. J.*, 1986, **237**, 175–180.
40 D. T. Nguyen, T. H. Le and T. T. T. Bui, *Eur. J. Med. Chem.*, 2013, **60**, 199–207.
41 A. Claiborne, *Handbook of Methods for Oxygen Radical Research. Catalase activity*, CRC Press, Inc, Boca Raton, FL, 1985.
42 J. Mohandas, J. J. Marshall, G. G. Duggin, J. S. Horvath and D. J. Tiller, *Cancer Res.*, 1984, **44**, 5086–5091.
43 K. Yanagimoto, K.-G. Lee, H. Ochi and T. Shibamoto, *J. Agric. Food Chem.*, 2002, **50**, 5480–5484.
44 M. Spiegel, K. Kapusta, W. Kołodziejczyk, J. Saloni, B. Żbikowska, G. A. Hill and Z. Sroka, *Molecules*, 2020, **25**, 3088.
45 L. Racané, L. Ptiček, G. Fajdetić, V. Tralić-Kulenović, M. Klobučar, S. K. Pavelić, M. Perić, H. Č. Paljetak, D. Verbanac and K. Starčević, *Bioorg. Chem.*, 2020, **95**, 103537.
46 M. Cindrić, I. Sović, M. Mioč, L. Hok, I. Boček, P. Roškarić, K. Butković, I. Martin-Kleiner, K. Starčević and R. Vianello, *Antioxidants*, 2019, **8**, 477.
47 E. N. Djuidje, S. Sciabica, R. Buzzi, V. Dissette, J. Balzarini, S. Liekens, E. Serra, E. Andreotti, S. Manfredini and S. Vertuani, *Bioorg. Chem.*, 2020, **101**, 103960.
48 M. C. Egbujor, J. Garrido, F. Borges and L. Saso, *Mini-Rev. Org. Chem.*, 2023, **20**, 190–209.
49 S. A. Güngör, İ. Şahin, Ö. Güngör, T. T. Tok and M. Köse, *Chem. Biodiversity*, 2022, **19**, e202200325.
50 İ. Gulcin and S. H. Alwasel, *Processes*, 2023, **11**, 2248.
51 N. Liang and D. D. Kitts, *Molecules*, 2014, **19**, 19180–19208.
52 B. Ou, D. Huang, M. Hampsch-Woodill, J. A. Flanagan and E. K. Deemer, *J. Agric. Food Chem.*, 2002, **50**, 3122–3128.
53 P. Yadav, B. Parshad, P. Manchanda and S. K. Sharma, *Curr. Top. Med. Chem.*, 2014, **14**, 2552–2575.
54 K. Chand, A. Hiremathad, M. Singh, M. A. Santos and R. S. Keri, *Pharmacol. Rep.*, 2017, **69**, 281–295.
55 E. M. Espinoza, J. A. Clark, J. B. Derr, D. Bao, B. Georgieva, F. H. Quina and V. I. Vullev, *ACS Omega*, 2018, **3**, 12857–12867.
56 S. Shi, H. Wang, J. Wang, Y. Wang, X. Xue, Z. Hou, G.-D. Yao, X.-X. Huang, H. Zhao and Q. Liu, *Bioorg. Chem.*, 2020, **100**, 103917.
57 Z. Sang, K. Wang, X. Han, M. Cao, Z. Tan and W. Liu, *ACS Chem. Neurosci.*, 2018, **10**, 1008–1024.
58 M. S. Nadeem, J. A. Khan and U. Rashid, *Int. J. Biol. Macromol.*, 2021, **193**, 19–26.
59 S. Manzoor, M. T. Gabr, B. Rasool, K. Pal and N. Hoda, *Bioorg. Chem.*, 2021, **116**, 105354.
60 M. A. Javed, M. S. Jan, A. M. Shbeer, M. Al-Ghorbani, A. Rauf, P. Wilairatana, A. Mannan, A. Sadiq, U. Farooq and U. Rashid, *Biomed. Pharmacother.*, 2023, **159**, 114239.
61 M. Shahid Nadeem, J. Azam Khan, I. Kazmi and U. Rashid, *ACS Omega*, 2022, **7**, 9369–9379.